JOURNAL OF GEOPHYSICAL RESEARCH, VOL. 104, NO. A6, PAGES 12,263–12,287, JUNE 1, 1999

Characteristics of pseudobreakups and substorms observed in the ionosphere, at the geosynchronous orbit, and in the midtail

A. T. Aikio,[1] V. A. Sergeev,[2] M. A. Shukhtina,[2] L. I. Vagina,[2]
V. Angelopoulos,[3] and G. D. Reeves[4]

Abstract. We present a comprehensive study of a sequence of two substorms and multiple pseudobreakups using optical, magnetic and incoherent scatter radar measurements, energetic particles from two geosynchronous satellites and particle and field data from the Geotail spacecraft located at $X_{gsm} \sim -86\ R_E$. Following conventional nomenclature, we classified as pseudobreakups those auroral breakups which did not exhibit significant poleward expansion ($< 2°$ magnetic latitude). Auroral intensifications following substorm breakups were also observed, and were classified separately. Pseudobreakups were found not to differ from substorm breakups in longitudinal extent (from 1.3 to 6.1 hours of magnetic local time), or in duration (from 5 to 16 minutes). In general, the ionospheric currents producing ground magnetic disturbances were more intense during substorms than pseudobreakups. We found that pseudobreakups are associated with the same magnetospheric processes as substorm breakups which involve current wedge formation, midlatitude magnetic Pi2 pulsations and energetic particle injections at the geosynchronous altitude. Moreover, pseudobreakups are associated with magnetic reconnection in the near–Earth region, evidenced by the typical subsequent detection of a plasmoid at Geotail. This implies that the magnetotail volume influenced by a pseudobreakup is quite large in radial distance. We conclude that there is no definitive qualitative distinction between pseudobreakups and substorms but there is a continuum of states between the small pseudobreakups and large substorms.

1. Introduction

Auroral activity in the nightside ionosphere can evolve in many different ways. The isolated substorm is the most sought after and studied evolutionery type of auroral activity. Other types are, e.g., substorm sequences, multiple onset substorms and pseudobreakups. In a review paper, *McPherron* [1979] argued that a sequence of substorms should be called a multiple onset substorm if successive onsets are so close to each other that the aurora has no time to move equatorward after each onset. Pseudobreakups were described as weak substorms, which may be associated with arc brightening but no poleward expansion. More recently, *McPherron* [1991] characterized pseudobreakups as short–lived (5 - 10 min), highly localized, weak ground magnetic perturbations.

Though existing a long time in the literature, pseudobreakups have been rarely studied using both ground and space observations. In the event studied by *Koskinen et al.* [1993] a pseudobreakup was associated with a dipolarization and a particle injection in the plasma sheet as well as a westward electrojet (WEJ) intensification and a Pi2 burst in the ionosphere. A weak, wedge–like current system was established, which did not expand. Weak activity was observed simultaneously over several hours of magnetic local time. Koskinen et al. concluded that the main difference between pseudobreakups and substorm breakups lies in their strength and consequences; they suggested that further comprehensive analysis of pseudobreakups should be performed.

In the events studied by *Nakamura et al.* [1994] pseudobreakups remained highly localized within several hundred kilometers in longitude in the ionosphere.

[1]Department of Physical Sciences, University of Oulu, Oulu, Finland
[2]Institute of Physics, University of St. Petersburg, St. Petersburg, Russia
[3]Space Sciences Laboratory, University of California, Berkeley
[4]Los Alamos National Laboratory, Los Alamos, New Mexico

Copyright 1999 by the American Geophysical Union.

Paper number 1999JA900118.
0148-0227/99/1999JA900118$09.00

The auroral structures associated with pseudobreakups resembled the major expansion aurora, except in their spatial scale. No significant WEJ activity was detected in association with pseudobreakups, but in some cases a counterclockwise current loop was observed. Slight change from taillike to dipolelike field configuration and particle injections were observed for some of the cases at the geosynchronous orbit. Nakamura et al. pointed out that although the entire expansion process takes longer for a major expansion onset, it consists of a number of injections and expansions, each with timescales of 2 - 8 min, comparable to those of pseudobreakups. They concluded that the major difference between pseudobreakups and substorm onsets is the number of occurences, the intensity and the scale size of the magnetospheric source.

Ohtani et al. [1993] studied a pseudobreakup, which produced small negative bays on the ground. They found that the current disruption producing dipolarization started in a very localized region in the magnetotail near 8.8 R_E and its magnitude decreased markedly as the disruption region expanded tailward. It was suggested that the spatial distribution of magnetic distortion before onsets determines the expansion scale of the current disruption. Ohtani et al. inferred that the absence of global expansion is the major difference between pseudobreakups and substorms and not the scale of the onset region in the magnetosphere.

Pulkkinen [1996] defined pseudobreakups as magnetospheric activations that produce relatively short–lived and often localized magnetic (0 - 100 nT) and auroral disturbances but no large–scale magnetotail reconfiguration.

The magnetic reconnection process is generally discussed as one of the basic mechanisms of a substorm expansion phase. Reconnection in the near–Earth tail is believed to commence at the expansion phase onset [*Hones,* 1979] or late in the growth phase [*Baker et al.,* 1996]. As reconnection continues, lobe field lines start to reconnect and a closed loop plasmoid is ejected downtail.

No systematic search of plasmoids in association with pseudobreakups have yet been done, altough one such event was recently demonstrated by *Petrukovich et al.* [1998]. In this paper we will elucidate characteristics of pseudobreakups in distinction to substorms in the ionosphere, at the geosynchronous orbit and in the midtail ($X_{gsm} \sim -86\ R_E$). Special attention will be paid to study of plasmoid signatures.

No definition of a pseudobreakup exists, though it is generally thought that pseudobreakups are rather short–lived and weak events and they are accompanied by a relatively small ionospheric expansion. We will use the following criterion to classify the events: pseudobreakups are not associated with a significant ($> 2°$) poleward expansion. In many cases, substorm breakups are followed by substorm intensifications. These will be studied separately from substorm breakups.

The long sequence of pseudobreakups, substorm breakups and intensifications occurred between 2000 and 2300 UT on January 18, 1993. The sequence included two substorms. Several pseudobreakups were observed between the major substorm expansions, as well as before the first substorm. No solar wind data were available for the event.

The instrumentation and the data analysis will be presented in section 2.1. Observations of the event characteristics in the ionosphere and at the geosynchronous altitude will be presented sections 2.2 - 2.5. The midtail dynamics in connection with the events is discussed in section 2.6. Finally, a summary and conclusions are given in sections 3 and 4.

2. Observations

2.1. Instrumentation and Data Analysis

High–latitude magnetic stations located at approximately along four longitudinal chains are utilized in this study: The KARA chain in Siberia, the IMAGE cross in Scandinavia and the Greenland Magnetometers along the east and west coasts of Greenland. Additional magnetic data were obtained from Ny Aalesund (NAL), Bear Island (BJN), Leirvogur (LRV), and Faroes (FAR) stations. The stations used in this study are shown in Figure 1. Stations cover a region from 39° to 159° Corrected Geomagnetic longitude (CGMlon) corresponding to a magnetic local time sector from 18.7 to 2.8 MLT at 2100 UT. These high–latitude magnetic data are used to monitor the development of electrojet currents.

The onset times of midlatitude Pi2 magnetic pulsations have been traditionally used to determine the

Table 1. SAMNET and Intermagnet Stations Used for SCW Calculation

Station	gglat	gglon	cgmlat	cgmlon
OTT	45.40	284.44	56.53	0.45
SJG	18.10	293.80	28.86	9.60
HAD	51.00	355.50	47.77	75.18
GML	57.16	356.32	54.98	78.24
YOR	53.95	358.95	50.98	78.97
CLF	48.02	2.27	43.52	79.65
HER	-34.43	19.23	-42.32	82.05
KVI	59.50	17.63	56.02	96.32
NUR	60.51	24.66	56.80	102.56
CZT	-46.43	51.86	-53.15	105.88
BOX	58.03	38.98	53.44	114.33
PAF	-49.35	70.26	-58.43	121.75
AMS	-37.80	77.57	-49.07	138.18
KAK	36.23	140.18	28.92	211.38
MMB	43.90	144.20	36.72	215.04
TUC	32.20	249.20	39.89	313.99
BOU	40.10	254.80	49.19	318.98

Here gglat and gglong refer to geographic latitude and longitude, respectively; cgmlat and cgmlong refer to corrected geomagnetic latitude and longitude.

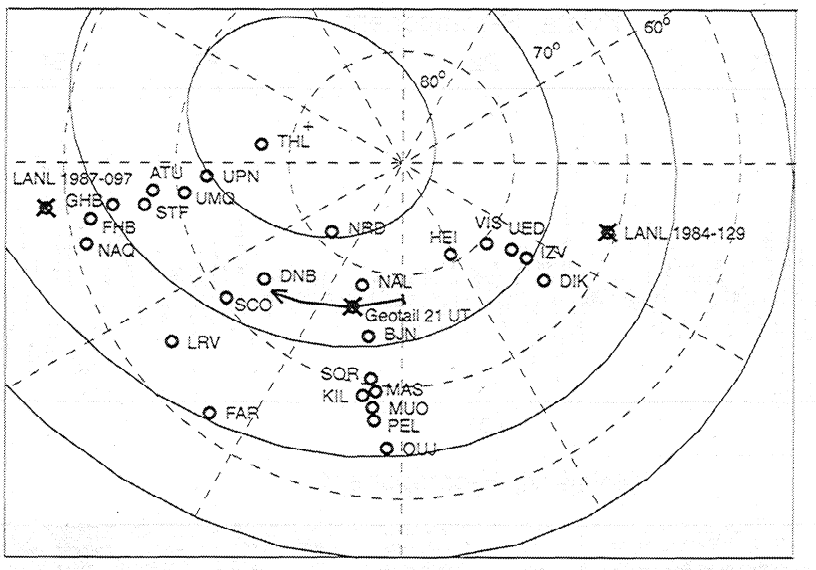

Figure 1. Magnetic high–latitude ground stations and the footpoints of S/C 1984–129 and S/C 1987–097. The footpoint of Geotail between 2000 and 2230 UT is shown by a solid line. Corrected geomagnetic (geographic) latitudes are shown by solid (dashed) lines.

times of substorm onsets [*Rostoker et al.*, 1980]. In this study we use two stations from the UK Sub–Auroral Magnetometer Network (SAMNET), Kvistaberg (KVI) and York (YOR) and both H and D components (see the location of stations in Table 1). In all the cases studied the onset times were the same at the two stations and in both components.

Bursts of irregular pulsations (PiBs) are studied from two Scandinavian high–latitude stations, Kilpisjärvi (KIL) and Ivalo (IVA), located at (65.8°, 104.5°) and (65.0°, 109.3°), respectively, in the CGM coordinate system. The CGM coordinate system is used if not otherwise indicated. The PiB pulsations correlate well with local auroral intensifications [*Bösinger et al.*, 1981].

During the events studied a special EISCAT auroral campaign was running providing a versatile data base from Northern Scandinavia. Optical data were measured by all–sky cameras at KIL (20–s resolution) and Muonio (MUO) (1–min resolution), auroral TV cameras at Esrange (ESR, 65.3°, 100.4°) and Porojärvi (POR, 65.9°, 105.1°) and a meridian scanning photometer at ESR (see also Figure 1). Local ionospheric measurements of plasma parameters were made by the EISCAT incoherent scatter radar at TRO (66.5°, 103.7°). The EISCAT measurements are used to derive the ionospheric electric field and conductances.

Midlatitude magnetograms from the SAMNET and the Intermagnet networks (Table 1) are used to calculate the substorm current wedge (SCW) location at the onset time of some of the events. The method is based on an inversion algorithm of midlatitude magnetic data and the model current system includes three components: substorm current wedge, partial ring current, and symmetric ring current (for details, see *Sergeev et al.* [1996] and *Vagina et al.* [1996]).

Geosynchronous particle data were obtained by two satellites, spacecraft (S/C) 1984–129 located in the morning and S/C 1987-97 in the evening sector (see the approximate footpoint locations in Figure 1). It is assumed that the particle injection occurs simultaneously at all energies in a limited region around midnight and after the impulsive injection electrons drift eastward and protons westward under the gradient–curvature drift. The onset time of a particle injection is calculated by using the energy dispersion of the flux increases. Then the particles at a given energy are traced back in a model magnetic field (T89) until the injection onset time to obtain the location of the injection boundary. This is done separately for the proton injections observed in the evening sector by S/C 1984–129, which provides the injection region western boundary and for the electron injections observed in the morning sector by S/C 1984–129, which provides the injection region eastern boundary.

Midtail observations ($X_{gsm} \sim -86\ R_E$, $Y_{gsm} \sim 4\ R_E$, $Z_{gsm} \sim -4\ R_E$) were provided by the Geotail satellite, which was located very close to the magnetic midnight (23.9 MLT), so its location was very favorable to see the effects of substorms. The approximate footpoint location is calculated using the T87L model and is shown in Figure 1. The Magnetic Field (MGF) and Energetic Particle and Ion Composition (EPIC) instruments are used to identify plasmoids.

2.2. Pseudobreakups During the Growth Phase of the First Substorm

2.2.1. General. The growth phase of the first substorm (hereafter substorm S1) took place from 2000 to 2053 UT on January 18, 1993. During this time inter-

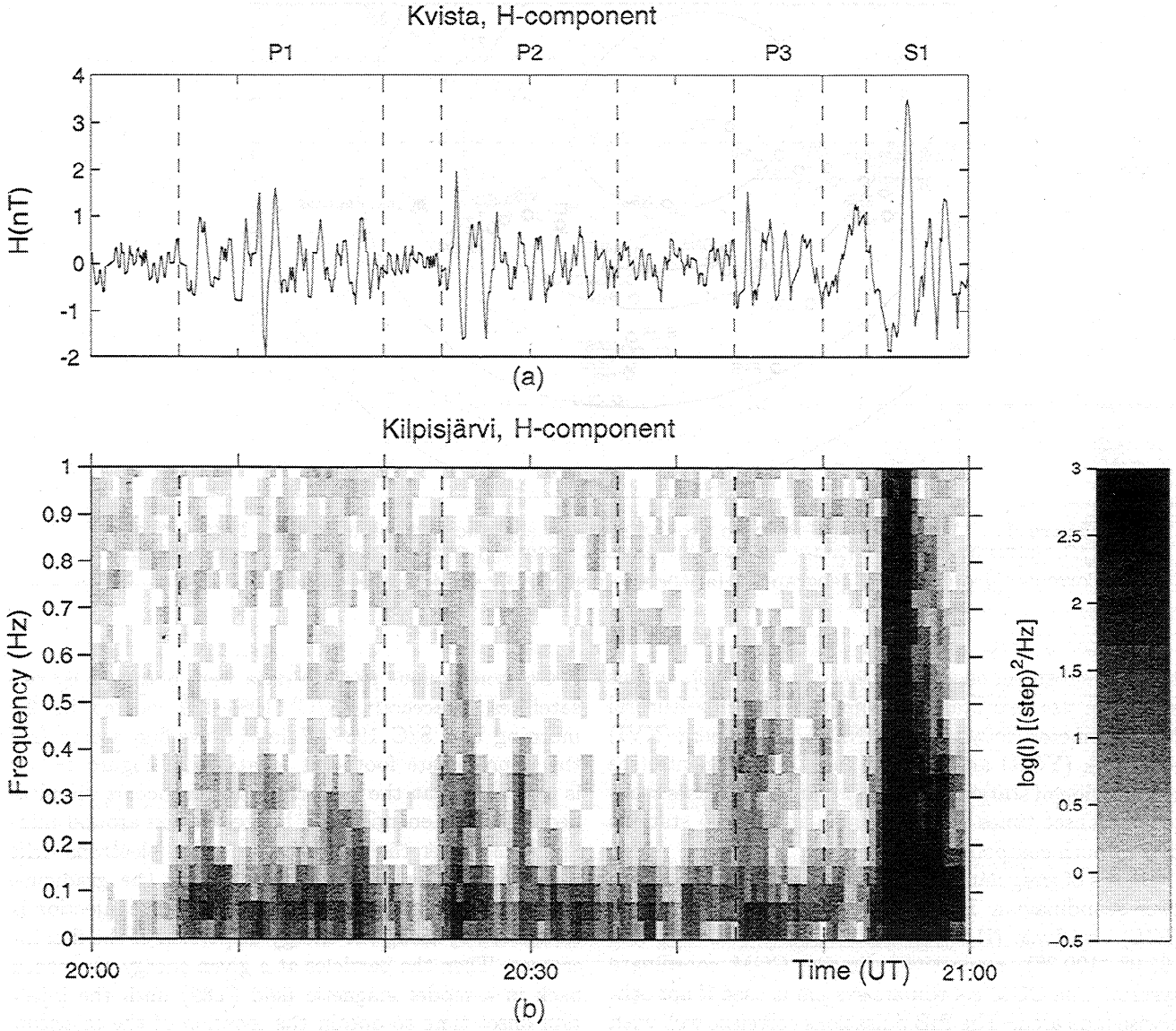

Figure 2. (a) High-pass filtered (T< 5 min) time series of KVI H component and (b) dynamic spectrum of KIL H component from 2000 to 2100 UT. Dashed vertical lines indicate onset and end times of Pi2 pulsations associated with pseudobreakups (P), substorm breakups (S), and substorm intensifications (I).

val, Scandinavia was located in the premidnight sector (22.8 – 23.7 MLT at KIL). A detailed study of the ionospheric conditions in the Scandinavian sector during the growth and expansion phases of the first substorm were presented by *Aikio and Kaila* [1996].

2.2.2. Magnetic pulsations. Figure 2a displays the midlatitude Pi2 magnetic pulsations in the H component from KVI, and Figure 2b shows bursts of irregular magnetic pulsations (PiBs) as can be seen from the dynamic spectrum of the KIL magnetic H component. The Pi2 pulsations showed four onsets, at 2006, 2024, 2044 and 2053 UT. The three first events are pseudobreakups (denoted as P1 - P3), and the last one is a substorm breakup (S1). The durations of Pi2 trains (marked by vertical dashed lines in Figure 2) and the PiB activity corresponded well to each other, and they were as follows: 2006 - 2020 UT (P1), 2024 - 2036 UT (P2), and 2044 - 2049 UT (P3).

2.2.3. Optical. The main optical features during the growth phase of substorm S1 were presented by *Aikio and Kaila* [1996] in Figures 2 and 3. Here we summarize the optical data by showing a plot of the intensity of the 427.8–nm auroral emission measured by a scanning photometer, which was located at Esrange (Plate 1). The geographic latitudes have been calculated from the elevation angles by assuming a height of 110 km for the altitude of the 427.8–nm emission. Unfortunately, in this plot utilizing a linear scale in intensity the northern arc is not properly visible, since it was much fainter than the southern arc. The start and stop times of Pi2 activity are marked by vertical dashed lines in Plate 3.

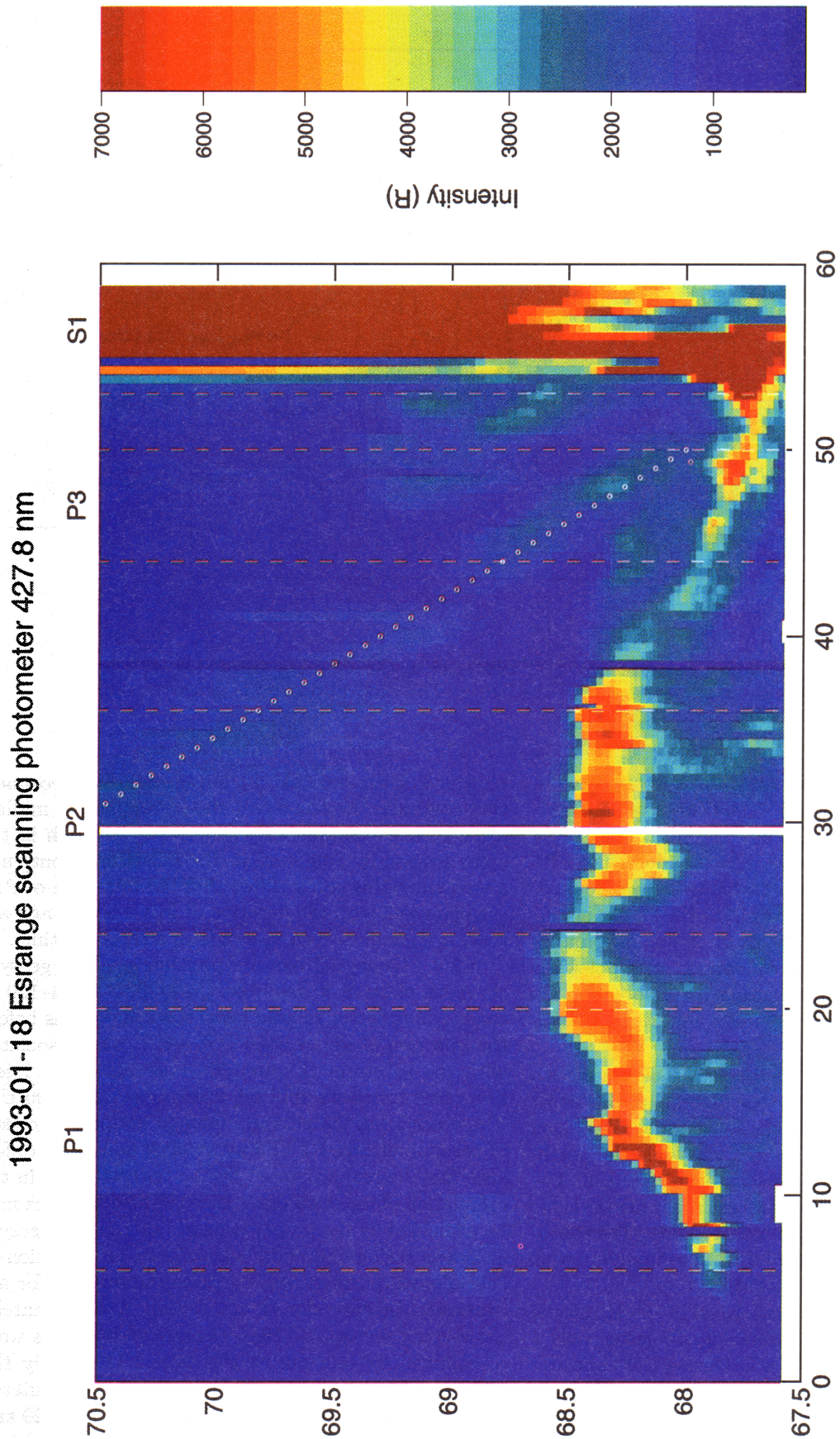

Plate 1. Arc locations and intensities measured from the 427.8–nm auroral emission by a scanning photometer at Esrange, Scandinavia, from 2000 to 2100 UT. White areas are data gaps and black vertical lines are background measurements. Dashed vertical white lines mark the duration of events as in Figure 2. The dotted line shows approximately the location of the northern arc between 2130 and 2150 UT.

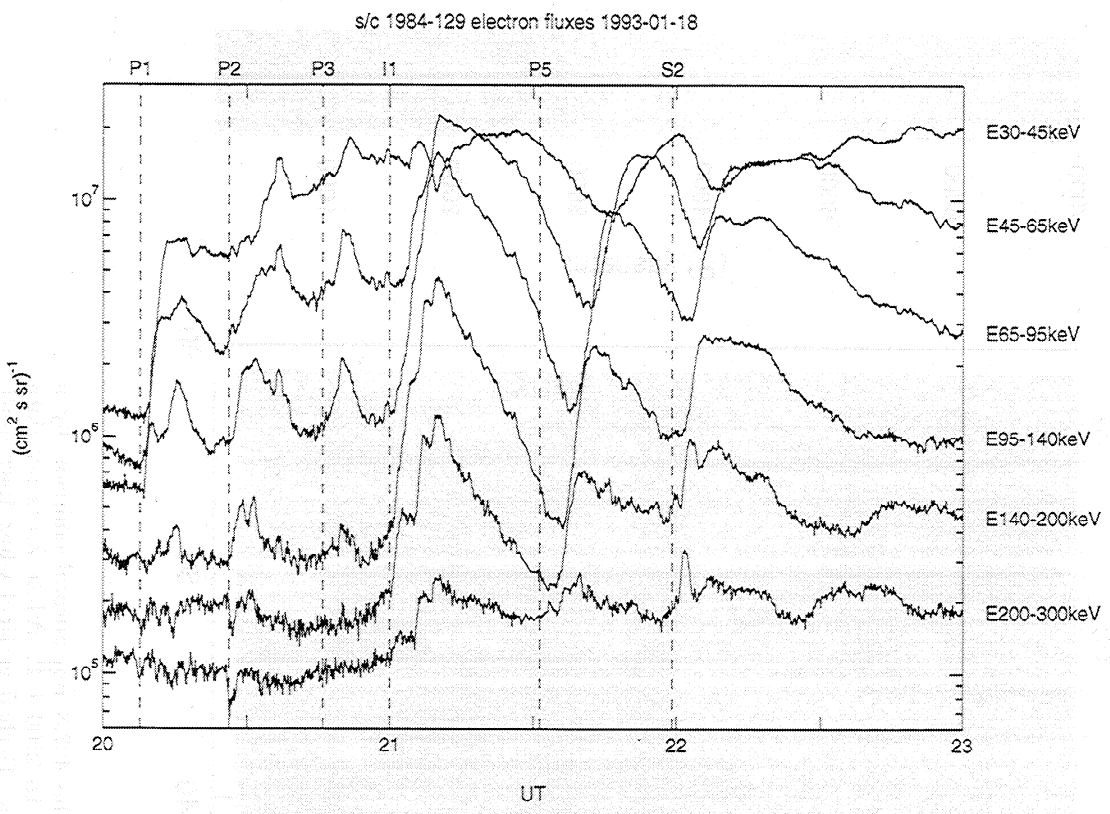

Figure 3. Electron fluxes measured by S/C 1984–129 in the morning sector for six energy channels displayed on the right–hand side of the figure. The vertical dashed lines correspond to the calculated onset times of the flux increases.

At about 2000 UT, two faint auroral arcs appeared in the sky, the southern one at 67.8° GGlat or 64.4° CGMlat (almost overhead MUO) and the northern one at 70.0° GGlat or 66.6° CGMlat. At pseudobreakup P1 onset the arcs intensified and started to move poleward. The poleward motion stopped at 2010 UT for the northern arc and at 2020 UT for the southern arc, in conjunction with the Pi2 activity termination. The poleward motion for both of the arcs during pseudobreakup P1 was about 0.7° of latitude (see also Figure 3 of *Aikio and Kaila* [1996]).

A second intensification of the arcs took place with a delay of about 1 min after pseudobreakup P2 onset at 2024 UT. The location of the southern arc remained rather stable during pseudobreak P2, while the northern arc started to drift equatorward at 2030 UT. The approximate location of the northern arc is made visible in Plate 3 by marking it with a dotted line. The southern arc started an equatorward drift in conjunction with the pseudobreakup P2 end at 2036 UT.

After 2042 UT multiple arcs formed in the vicinity of the existing arcs. The pseudobreakup P3 lasted only 5 min and commenced at 2044 UT. During this time arcs intensified while they were drifting equatorward. Only 3.5 min after pseudobreakup P3 cessation the substorm S1 onset took place.

In all the studied events Pi2 pulsations correlated well with auroral brightenings, which lasted ≤ 1.5 min longer than the associated Pi2 activity (see Plate 3). *Singer et al.* [1988] suggested that while the near–tail reconnection continues, Alfvén waves and subsequently midlatitude Pi2s are continuously generated. Though in the cases studied by Singer et al. the pulsations continued a long time, this study shows that the duration of Pi2s correlate well with the duration of PiB activity and auroral brightenings even in events of a short lifetime.

2.2.4. Geosynchronous particles. The geosynchronous electron fluxes observed at S/C 1984–129 in the morning sector showed three clear injections before the injection at about 2100 UT, which was associated with the substorm (Figure 3). The calculated injection onset times are 2007:50, 2026:20 and 2046:00 UT. These times lag the ground midnight sector Pi2 onsets of pseudobreakups P1 - P3 by about 2 min. The difference may be real or caused by the uncertainties in the calculation of injection onset times. The difference may be explained by the propagation of flows to the geosynchronous region that take longer than propagation of field–aligned currents and particles responsible for activations [*Angelopoulos et al.*, 1996a]. Unfortunately, the evening sector S/C 1987-97 particle detectors were contamined by Sun during this time. Thus only the injection region eastern boundaries could be calculated from the electron fluxes measured by S/C 1984–129 and they appear to originate close to the satellite and just east of the KARA magnetic station chain in Siberia, i.e., at 2.2, 2.6 and, 2.6 MLT, respectively.

2.2.5. High–latitude magnetograms. Study of

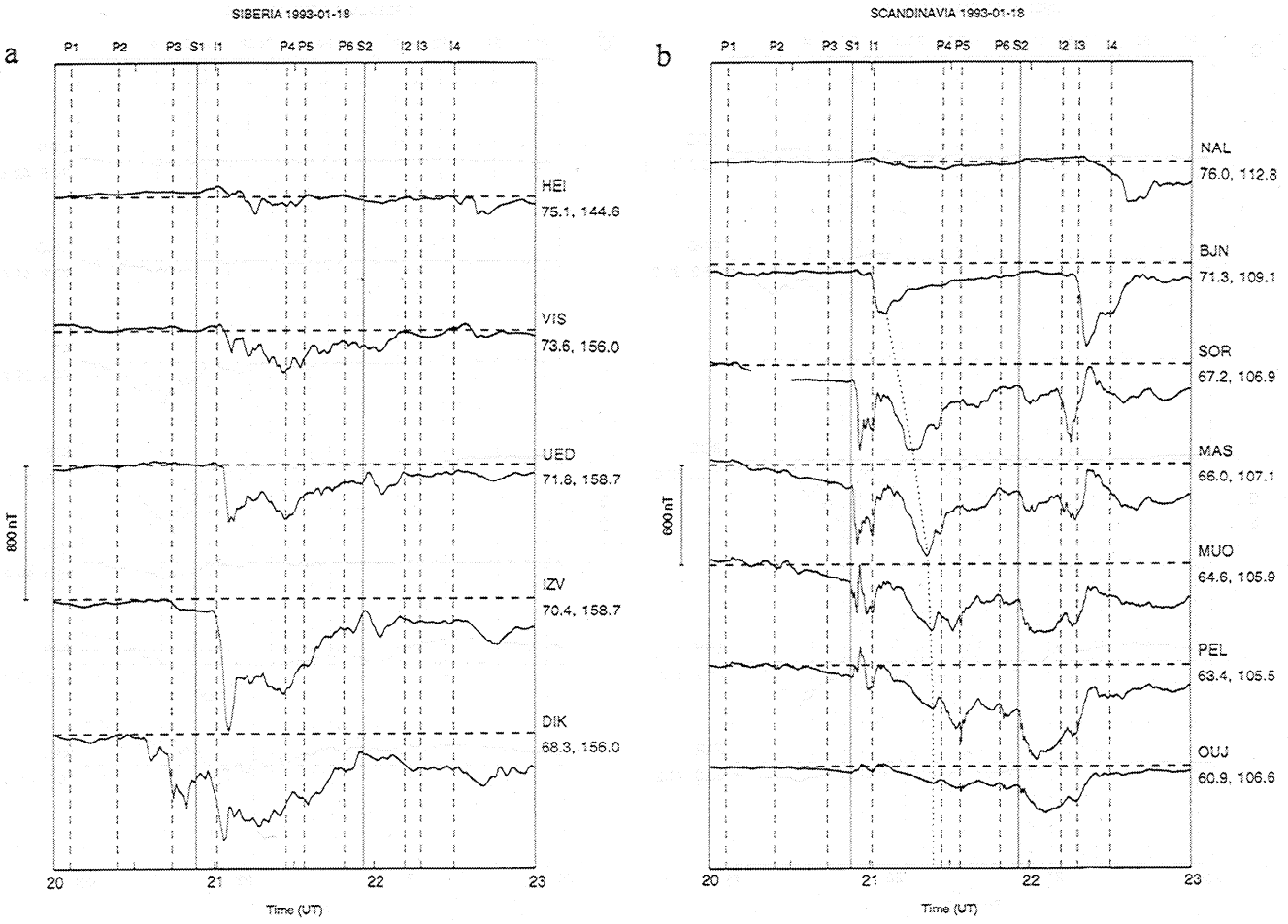

Figure 4. Magnetic north–south components from four different local time sectors: (a) KARA chain in Siberia, (b) selected stations of the IMAGE cross in Scandinavia, NAL and BJN, (c) Greenland east coast stations, LRV and FAR, (d) Greenland west coast stations. Corrected geomagnetic latitude and longitude values are shown under the name of a station. Pseudobreakups (P) and substorm intensifications (I) are marked by a dashed line, substorms (S) by a solid line. The dotted line in Figure 5b indicates the perturbation produced by a southward drifting double arc.

magnetograms from the Scandinavian sector (Figure 4b) indicates that arc intensifications produced small ($\leq$ 50 nT) positive peaks in the X component and they could be resolved only by the stations located close to the southern arc (MAS, MUO and PEL). Since the convection electric field was northward in the vicinity of the southern arc according to the EISCAT measurement [*Aikio and Kaila*, 1996], arc intensifications were expected to produce enhancements of the eastward current in the vicinity of the arc, thereby causing positive disturbances in the horizontal magnetic component.

The most equatorward station of the Siberian chain, DIK (68.3° CGMlat), recorded a minor negative bay (30 nT) during pseudobreakup P1 (Figure 4a). Steep negative bays commenced at 2033 and 2043 UT and the first of these occurred during pseudobreakup P2, so it is possible that the disturbance started at latitudes lower than DIK and then expanded poleward. The beginning of a negative bay at 2043 UT occurred in coincidence with the onset of pseudobreakup P3 within 1 min and the bay reached 450 nT at 2049 UT. To be classified as a substorm breakup, the event should be associated with a poleward expansion of at least 2° in latitude according to a definition given in Introduction. Owing to insufficient data it is impossible to deduce the exact amount of poleward expansion in the morning sector and we classify events P2 and P3 as pseudobreakups.

No magnetic perturbations in the evening sector were associated with pseudobreakups P1 - P3.

2.2.6. SCW locations. The substorm current wedge calculation on the basis of midlatitude magnetograms provides the following extensions for pseudobreakups, P1: 2238 - 0029 MLT (width 1.9 MLT), P2: 2252 - 0324 MLT (4.5 MLT) and P3: 2328 - 0231 MLT (3 MLT). To facilitate the comparison of the onset region locations determined by different methods, we present Figure 5. The eastern edge of the SCW is located close to Siberian chain for pseudobreakups P2 and P3, in good accordance with geosynchronous injection eastern edge estimates. For pseudobreakup P1 the SCW eastern edge location is estimated to be between Siberia and Scandinavia, well westward of the injection

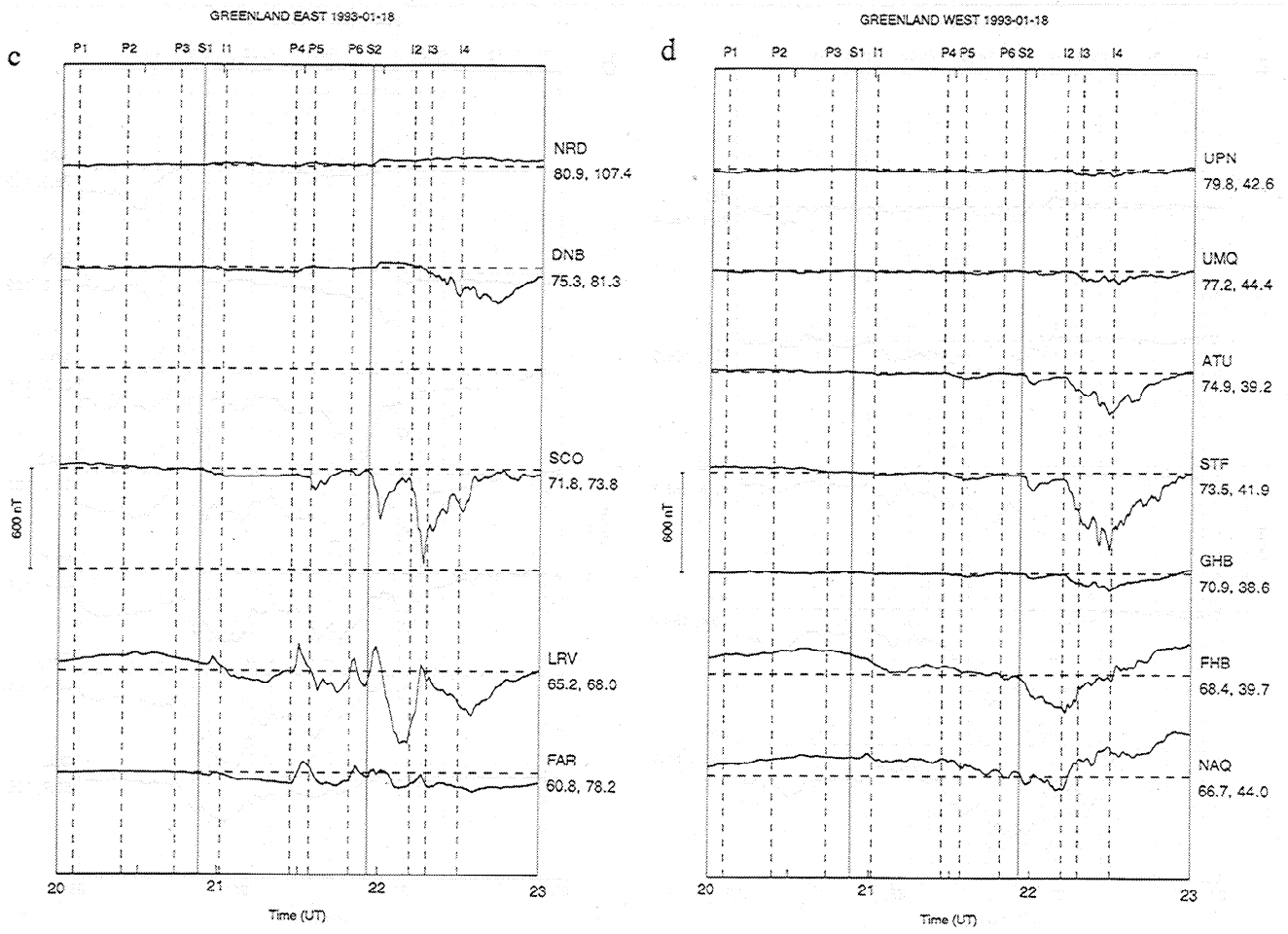

Figure 4. (continued)

region eastern edge estimate, but in accordance with Siberian sector chain magnetic data. The western edge locations of the SCW for events P1 - P3 are calculated to be just west of Scandinavia, but since no negative bays commence in association with these events, the SCW plausibly lies just eastward of the Scandinavian chain.

2.3. Substorm Breakup S1 and an Ensuing Intensification

2.3.1. Magnetic pulsations. Substorm S1 breakup was recorded by the Scandinavian sector stations at 2053 UT. The most equatorward arc brightened, there was a burst of very intense PiB pulsations, an onset of midlatitude Pi2 pulsations (Figure 2) and a VLF hiss emission (data not shown). A substorm intensification (I1) commenced at 2101 UT and it was coincident with a new onset of midlatitude Pi2 pulsations and a burst of PiB pulsations (Figure 6). The Pi2 activity continued until 2109 UT, which we take as the end of the expansion phase. After 2109 UT, auroral forms started to move equatorward.

2.3.2. Optical and EISCAT data. At substorm onset the most equatorward arc, located at 67.7° GGlat or 64.3° CGMlat, brightened explosively and started to move poleward (Plate 3). A westward traveling surge (WTS) appeared at the eastern horizon of the KIL all-sky camera at 2054 UT, moved rapidly over zenith and disappeared to the west in 40 s (see Figure 2 of *Aikio and Kaila* [1996]). The total poleward expansion of the auroral bulge associated with substorm breakup S1 was about 4° in latitude. The precipitation in the arcs at the boundary of the auroral bulge as well as in the arc inside the bulge were very energetic as estimated from the EISCAT radar measurements: the maximum values of the Pedersen (Σ_P) and Hall conductances (Σ_H) were 40 S and 214 S, respectively and $\Sigma_H/\Sigma_P = 5.4$ [*Aikio and Kaila*, 1996]. In coincident with substorm intensification I1 at t 2101 UT a brightening arc started to form in the northern horizon of the KIL all-sky camera.

2.3.3. High-latitude magnetograms. The substorm S1 breakup at 2053 UT was associated with commencements of steep negative bays in the Scandinavian sector (Figure 4b). The maximum disturbance of 500 nT was measured at SOR. The substorm intensification I1 at 2101 UT produced further poleward displacement of the WEJ activity as evidenced by a commencement of a new negative bay at BJN where it reached 300 nT at 2103 UT.

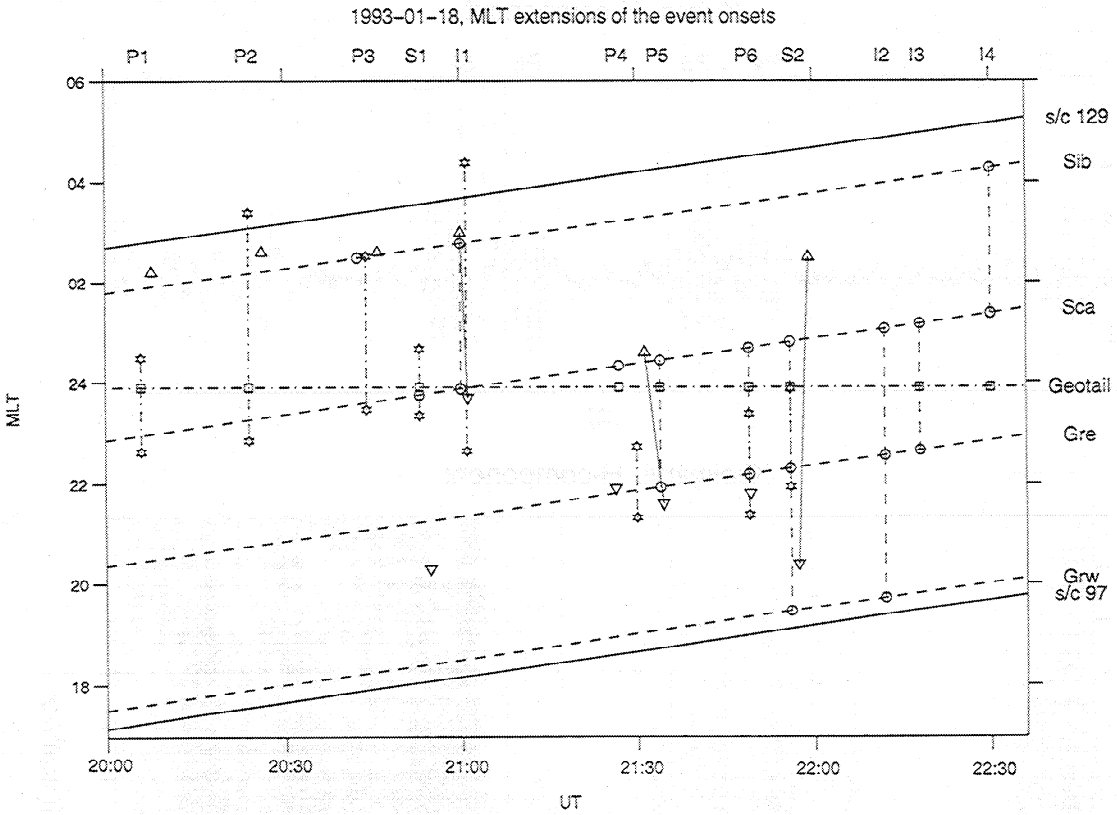

Figure 5. Extensions of the event onsets in UT–MLT coordinate system. The location of the S/C 1984–129 and S/C 1987–097 are shown by solid lines, the location of Geotail satellite by a dash–dotted line and station chains located in Siberia (Sib), Scandinavia (Sca), on the Greenland east (Gre) and west (Grw) coast by dashed lines. Triangles pointing up (down) display the injection region eastern (western) boundary and together they define injection source regions, which are marked by vertical solid lines. The ground sectors where a negative bay commences at the onset of an event are marked by circles and they are connected together by vertical dashed lines. Squares denote the onsets observed by Geotail. SCW locations calculated by midlatitude magnetometer data are shown by vertical dash–dotted lines bounded by stars.

In the morning sector at DIK the onset of a steep negative bay occurred 3 min after substorm breakup S1. At higher latitudes negative bays commenced in association with the substorm intensification I1 and the maximum disturbance of 800 nT was recorded at IZV (70.4° CGMlat). Poleward expansion of currents in the morning sector associated with substorm intensification I1 was about 3.5° (from DIK to VIS). In the evening sector no steep bays were observed, but in Iceland (LRV) and on the east coast of Greenland a weak WEJ started to flow after the onset of substorm S1.

2.3.4 Geosynchronous particles. The S/C 1984-129 in the morning sector measured a significant increase in electron fluxes at all energies up to 300 keV (Figure 3). The calculated injection onset time for the electrons is 2100:00 UT and the eastern edge of the injection region 3.0 MLT, i.e., again close to the Siberian chain. The injection onset time corresponds to the substorm intensification I1. The electron injection associated with substorm breakup S1 at 2053 UT took place outside of the drift shell where S/C 1984–129 was located.

The proton fluxes at S/C 1987–097 in the evening sector are displayed in Figure 7. Only the four lowest–energy channels are displayed to keep the figure readable, but in total six channels corresponding to energies up to 241 keV are used in the calculations. Associated with substorm breakup S1 the proton fluxes at S/C 1987–097 showed a pronounced injection which is traced back to 2054:40 UT and 20.9 MLT. The tracing of the proton injection in association with substorm breakup S1 gives a too western estimate of the injection western boundary, since optical observations show that the WTS formed to the east of Scandinavia. The next pronounced flux increase was associated with substorm intensification I1 and it is clearly dispersed. The estimated onset time is 2101:10 UT and location 23.7 MLT. The proton and electron injections related to the substorm intensification I1 define together an injection source region extending from 23.7 to 3.0 MLT (width 3.3 MLT).

2.3.5. SCW locations. The substorm current wedge at substorm breakup S1 is estimated to extend from 2320 to 0040 MLT (width 1.3 MLT), which puts it

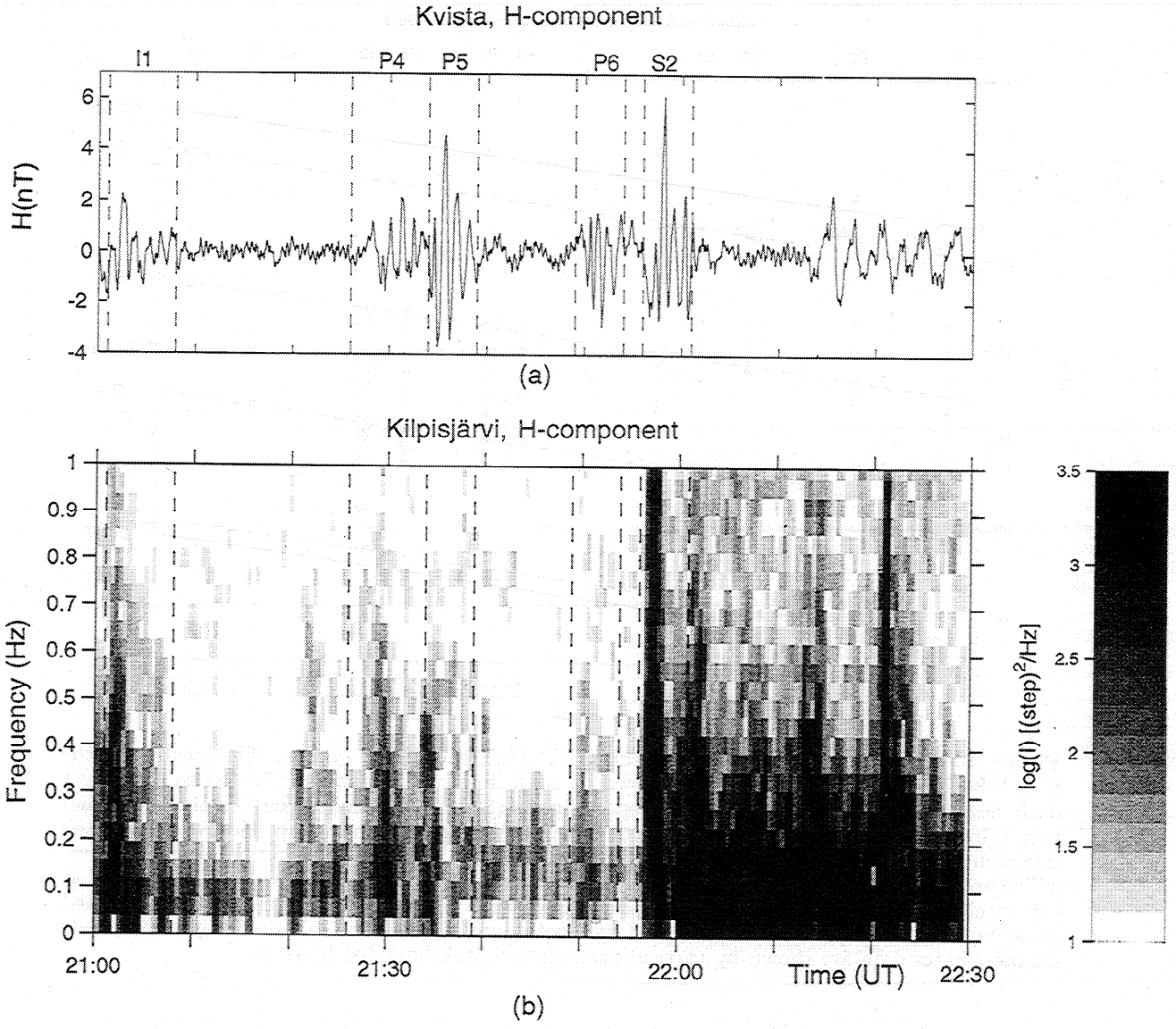

Figure 6. As Figure 2, but for a time interval of 2100 - 2230 UT.

in the Scandinavian sector. The width of the SCW associated with the substorm intensification I1 is much broader, 5.7 MLT, and the location is from 2240 to 0420 MLT, which is in good accordance with the injection region estimate (Figure 5). The SCW expands both eastward and westward in association with the substorm intensification, so that it encompasses the Siberian and Scandinavian chains, but does not quite reach the east coast of Greenland, which is in consistent with the high-latitude magnetic data.

2.4. Pseudobreakups Between the Two Substorms

2.4.1. Magnetic pulsations. Midlatitude Pi2s occurred during 2127 - 2134 UT (P4), 2134 - 2139 UT (P5), and 2149 - 2154 UT (P6) (Figure 6). Again, the PiB and Pi2 activity corresponded rather well to each other, though PiBs started earlier than the Pi2s associated with pseudobreakup P4. Pseudobreakups P4 and P5 followed each other with no clear separation but they can be distinguished by the increase in the Pi2 amplitude at pseudobreakup P5 onset.

2.4.2. Optical and EISCAT data. The expansion phase of substorm S1 lasted 16 min. The expansion phase was not followed by a recovery phase with a slow recovery of auroras to lower latitudes and decrease of magnetic activity to a quiet level in the midnight sector. Instead, an arc system consisting of two closely spaced arcs at the northern bulge boundary started a rapid equatorward drift at 2109 UT. The arcs are visible in the first frame of the collection of ASC figures, the top (bottom) 12 figures measured at MUO (KIL) are shown in Figure 8. Note, that the double arcs close to the horizon cannot be resolved by the cameras until about at 2113 UT. The equatorward drifting double arc produced a significant negative bay in the magnetic X component in the Scandinavian sector (Figure 4b, dot-

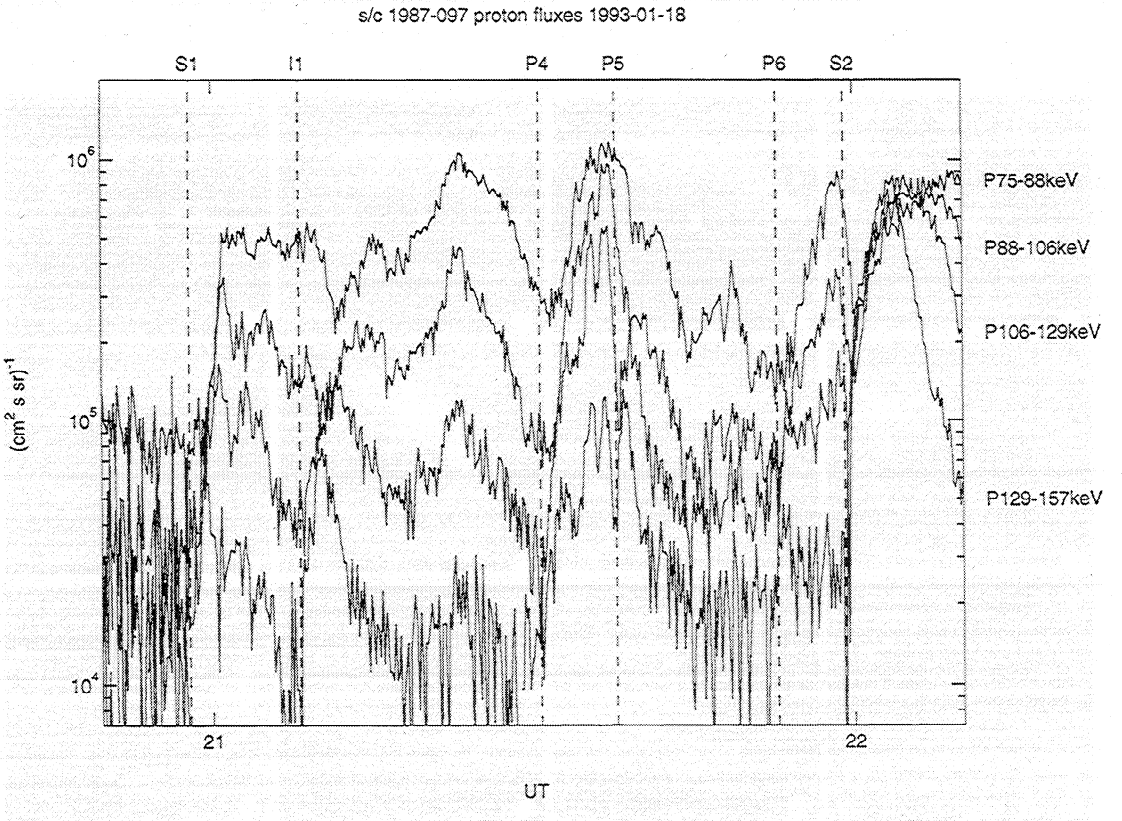

Figure 7. Proton fluxes measured by the S/C 1987–097 in the evening sector for the four lowest–energy channels displayed on the right–hand side of the figure. The vertical dashed lines correspond to the times of flux increases at the highest–energy channel displayed (129 - 157 keV).

ted line), which moved equatorward from BJN to MUO. Also, the zero crossing of the Z component drifted equatorward and it was observed close to the minimum of the H component, confirming the interpretation that the negative bay was really produced by a current system associated with the arc (data not shown). The maximum negative bay produced by the arc was 560 nT, which is comparable to substorm signatures. When the arc crossed the EISCAT beam at 2119 UT, a Hall conductance of 80 S and Σ_H/Σ_P= 2.3 was measured (Figure 9). The double peak in the second conductance enhancement occuring at 2124:30 UT was due to a fold forming in the northern arc of the double arc system. The high Hall–conductance combined with a southward electric field produced an intense westward Hall current within the arc system.

The fold developing in the poleward arc at 2124:20 UT disappeared to the east within 80 s (vaguely visible in Figure 8 by the MUO ASC, the fold was better seen by the KIL ASC). The pseudobreakup P4 onset time is 2127 UT according to Pi2 pulsation data. Optically, this was related to a small intensification occuring in the eastern horizon in the northern arc observed by KIL ASC at 2127:43 UT (not shown). The northern arc of the double arc system became fragmented at about 2128 UT and existed thereafter only in the eastern part of the sky. The other arc continued the equatorward drift.

The pseudobreakup P5 started at 2134 UT. Again, a small intensification was observed in the eastern part of the fragmented arc, and then a surge came from the east and moved slowly westward until about 2140 UT when the head was just over KIL. For comparison, the surge observed at 2140 UT by both of the MUO and KIL all–sky cameras is shown in Figure 8. Thereafter the surge started to retreat back eastward. The expansion of aurora produced by the surge was about the distance between MUO and KIL, i.e., 1.2° CGMLat, so the event fulfills the definition of pseudobreakup given in the introduction. The Pi2 activity lasted until 2139 UT, in relation with the westward movement of the surge.

The edge of the surge extended to TRO at 2140 UT, where the EISCAT radar measured Hall conductance enhancements up to 30 S (Figure 9). This is much less than for the WTS associated with substorm S1 or for the equatorward drifting arcs measured between 2116 and 2126 UT. The surge differed from the classical westward traveling surge also in the magnetic signatures. At stations under the surge head at 2140 UT (PEL - KIL), the X component was increasing, i.e., the surge was not associated with a westward current and a negative bay. The details of the current system associated with the pseudobreakup surge will be left for a future study and will not be discussed in more detail here.

At 2149 UT the arc was located just equatorward of MUO. In association with pseudobreakup P6 onset the arc started to brighten at 2150 UT and stayed bright

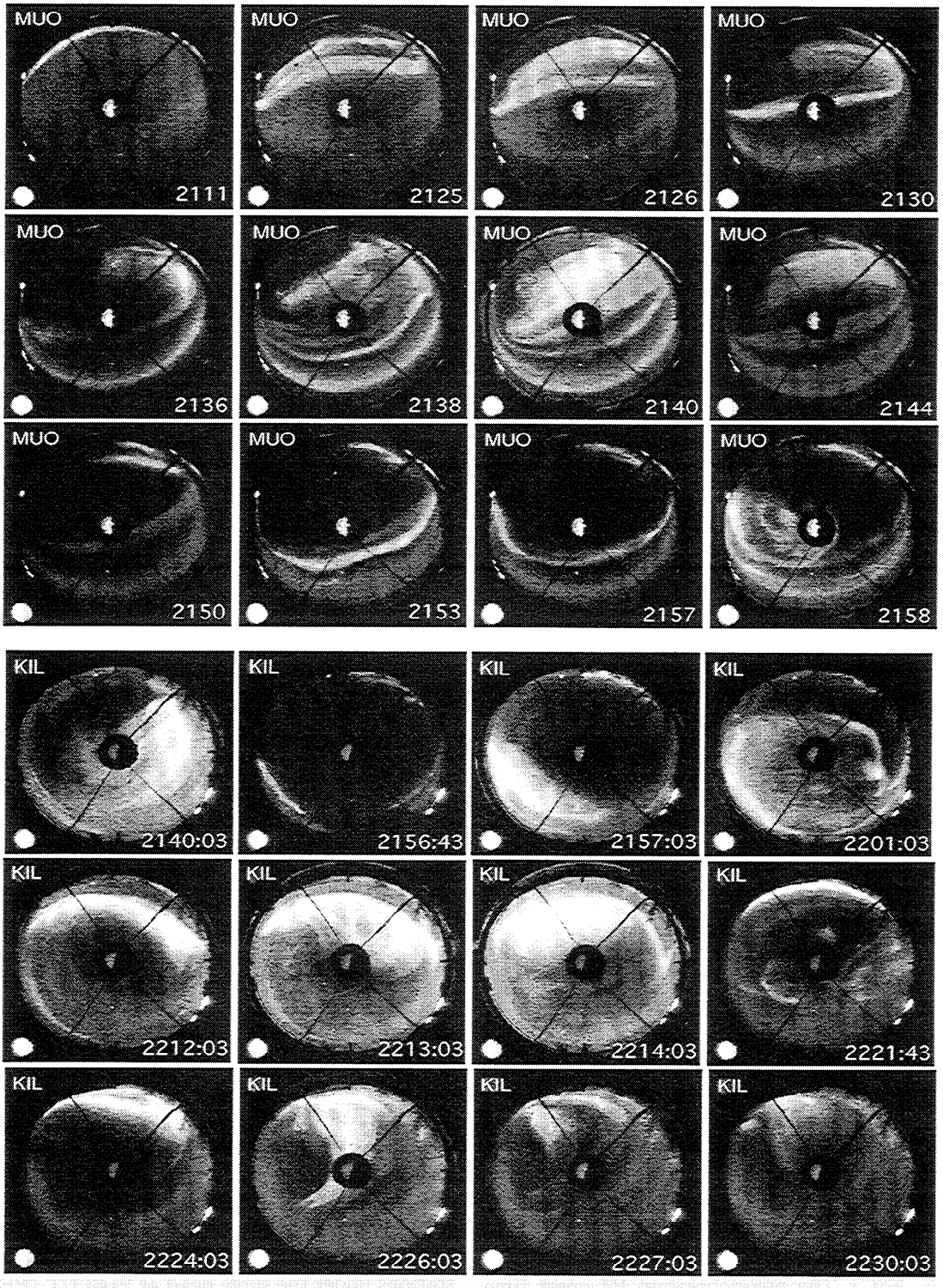

Figure 8. Collection of all-sky frames. First twelve frames are from MUO from time interval of 2111 - 2158 UT. Notice that the camera exposure time is longer at every ten minutes, so there is no intensification of the surge at 2140 UT. Rest twelve frames are from KIL from 2140:03 UT and from time interval of 2156:43 - 2230:03 UT. North (east) is located to the top (right) of the figure.

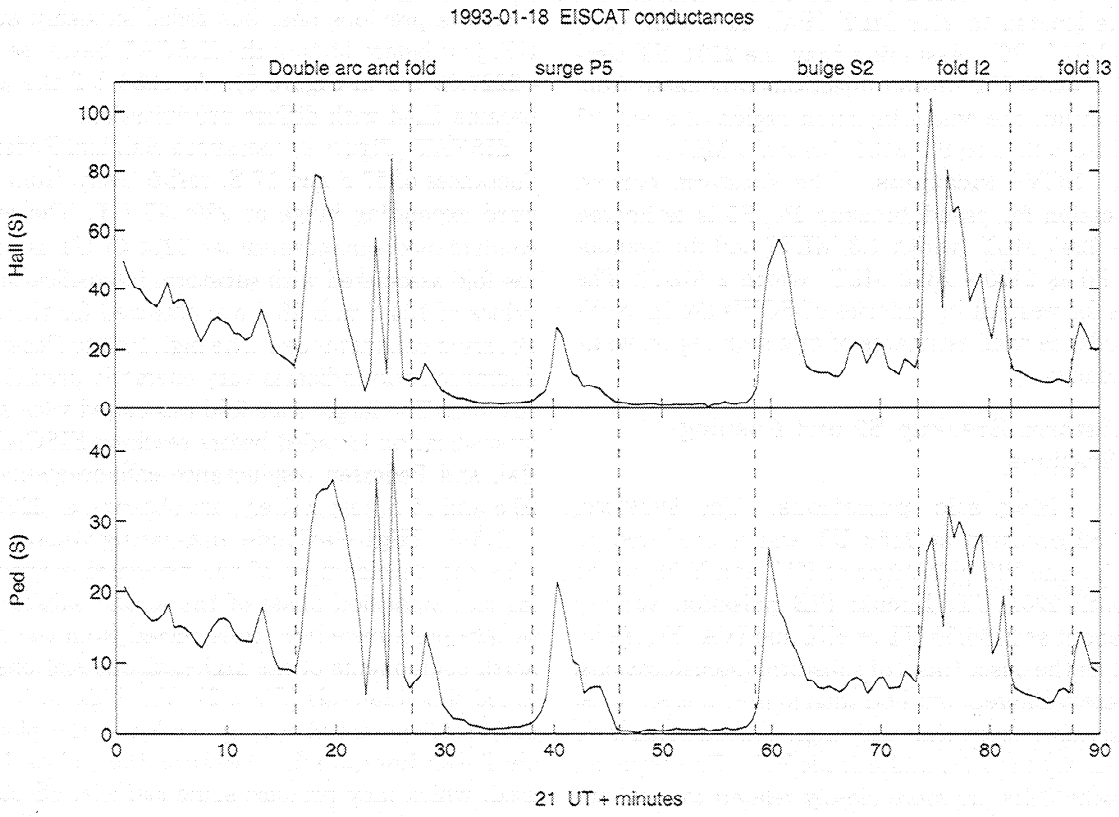

Figure 9. Height–integrated conductivies as measured by the EISCAT radar at Tromsø.

until 2155 UT, about one minute longer than the end of Pi2 activity associated with pseudobreakup P6. At 2156 UT the intensity of the arc had decreased somewhat and the onset of substorm S2 can be seen in the next frame taken at 2157 UT.

2.4.3. High–latitude magnetograms. After substorm breakup S1 and the subsequent intensification I1 an intense WEJ was flowing in the morning sector (Figure 4a). The WEJ started to decrease at all stations after 2126 UT showing substorm recovery phase type behaviour. No magnetic effects associated with the three pseudobreakups P4 - P6 were observed. The midnight and late evening sector magnetograms, however, exhibited substorm growth phase behavior. In the midnight sector (Scandinavia) a negative bay produced by the southward drifting double arc system was observed, as discussed previously in connection with optical observations. Pseudobreakups P4 - P6 could be identified at stations located in the vicinity of the arc system. In the discussion below, we measure the disturbances from the level prevailing at the start of the activation. At MUO, PEL and OUJ a decrease in the X component started at 2126 UT (P4) and was 190 nT at maximum. The 2134 UT onset (P5) was visible as a short–lived negative peak in the PEL and MUO magnetograms producing an additional disturbance of 120 nT. The pseudobreakup P6 produced a negative disturbance of 90 nT in the X components in Scandinavia. In the late evening sector (on the east coast of Greenland) the pseudobreakup P4 was associated with a positive disturbance at LRV and FAR. Pseudobreakup P5 produced negative bays of magnitude of about 100 nT at SCO, LRV and FAR. Pseudobreakup P6 was associated with a minor negative bay at SCO and positive peaks at lower latitudes. Pseudobreakups P4 - P6 were not associated with sudden changes in the currents flowing on the west coast of Greenland. The eastward electrojet (EEJ) was decreasing at the latitude of NAQ and a very weak WEJ flowed at high latitudes (STF and ATU) between pseudobreakups P4 and P6.

2.4.4. Geosynchronous particles. The morning sector geosynchronous S/C 1984–129 measured only one electron injection between the substorms (Figure 3). The calculated onset time of this injection is 2131:20 UT (P5) and the location 0.6 MLT. The evening sector S/C 1987–097 measured several proton flux enhancements between 2109 and 2156 UT (Figure 7). The proton flux enhancement starting after 2126 UT was very peculiar and altogether four peaks can be resolved. The timing was performed for the first and the last enhancement corresponding to times of 2126:20 UT (P4) and 2134:30 UT (P5). Pseudobreakup P6 was associated with flux enhancements only at the lowest energies and the calculated onset time was 2149:10 UT. The western edges of the source regions of these injec-

tions were located to 21.9 MLT (P4), 21.6 MLT (P5) and 21.8 MLT (P6). Assuming that the 2131 UT electron and 2134:30 UT proton injections originated from the same event, the whole injection region of event P5 extended from 21.6 to 0.6 MLT (width 3 MLT).

2.4.5. SCW locations. The substorm current wedge location for pseudobreakup P4/P5 is estimated as 2120 - 2240 MLT (width 1.3 MLT) and for pseudobreakup P6 as 2120 - 2320 MLT (width 2 MLT). The estimates for western boundaries of SCWs are in excellent accordance with estimates of injection region western boundaries.

2.5. Substorm Breakup S2 and Ensuing Intensifications

2.5.1. Magnetic pulsations. The substorm breakup S2 occurred at 2156 UT and it produced an onset of intense Pi2 pulsations at KVI and YOR which lasted until 2201 UT. Intense PiB pulsation activity started about at 2156:30 UT at KIL and IVA (Figure 6).

To define the onset times of substorm intensifications, we use here a different method than in previous sections, since it seems evident that very high–latitude onsets do not necessarily produce midlatitude Pi2s. Furthermore, auroral zone PiBs are more closely related to local auroral enhancements than to global very high latitude onsets. So, the onset times for substorm intensifications are determined on the basis of commencements of high latitude negative magnetic bays and we arrive at values of 2212 UT (I2), 2218 UT (I3), and 2230 UT (I4) (see Figure 4). Notice, that this method is not in contradiction with the definitions made in previous sections, but the onset time determination suffers from larger uncertainties, especially for the I4 onset time (a few minutes).

2.5.2. Optical and EISCAT data. The KIL all–sky camera measured an intensification starting at 2156:40 UT in the western part of the most equatorward arc (Figure 8). For comparison, the onset measured by the MUO all–sky camera at 2157 UT is also shown. The arc brightening was followed by an eastward and poleward expanding bulge. A bright arc formed at the boundary of the bulge at 2201 UT, which was related to the PiB burst observed at KIL. By 2207 UT the bulge had expanded to the northern horizon of the KIL ASC and a bright arc was left on the poleward boundary of the bulge. The poleward expansion of optical forms in association with substorm breakup S1 was about 3.6°. Substorm intensification I2 was associated with an appearance of a large–scale fold oriented equatorward of the arc at 2212 UT. The fold drifted westward (see 2212:03 - 2214:03 UT in Figure 8). The second substorm intensification, I3, started by brightening of the arc at the poleward boundary of the bulge at 2220 UT, which was associated with a PiB burst at KIL. A westward drifting fold appeared again in the arc at 2223 UT. This fold extended even further equatorward of the arc than the previous one, but faded suddenly at 2226:20 UT, just before hitting the EISCAT beam (see 2224:03 - 2227:03 UT in Figure 8). At 2230 UT the whole sky became filled with diffuse precipitation.

EISCAT (Figure 9) measured Hall and Pedersen conductances of 57 S and 17 S, respectively, from the eastward expanding bulge at 2200:45 UT. The next large conductance enhancement at 2214:45 UT is related to the fold associated with substorm intensification I2 and values of 104 S and 28 S are obtained for the Hall and Pedersen conductances. The high Hall to Pedersen conductance ratio indicates very energetic precipitation in the fold. The large–scale fold associated with substorm intensification I3 faded before reaching EISCAT, so the Hall and Pedersen conductance enhancements only to 29 S and 15 S, respectively, are observed at 2228:15 UT.

2.5.3. High–latitude magnetograms. To visualize the development of the westward electrojet during the expansion phase of the second substorm, color surface plots have been constructed from the magnetic north components of the high–latitude stations and selected time intervals (Plate 2). The high–latitude magnetic stations are shown by circles in the plots. Simple linear interpolation between the points has been used, which may produce some artificial effects due to the sparse distribution of the stations in the longitudinal direction. To include more data of the IMAGE chain stations, the data from the other local time sectors have been extended equatorward by assuming a constant value from the most equatorward station to the latitude of MUO, 64.6° CGMlat. This extrapolation affects most the Siberian sector; for the other local time sectors the effect is small.

Before the substorm breakup S2 the maximum of the WEJ was located at the latitude of PEL (63.4° CGMlat) in the midnight sector (Scandinavia) in the vicinity of auroral arcs (Plate 2a). Note that PEL is the circle equatorward of the colour surface at a longitude of 106°, so it has no effect on the plot. In the morning sector (Siberia) the WEJ had decreased to a small value and in the evening sector (Greenland) the magnetic north–south components were close to zero indicating very small electrojet intensities.

At substorm breakup S2 at 2156 UT the intensity of the WEJ enhanced in the midnight sector from PEL to SOR (63.4° - 67.2° CGMlat) and in the premidnight sector at SCO (71.8° CGMlat) while the EEJ intensified at lower latitudes (Plate 2b). A small enhancement of the WEJ occurred on the Greenland west coast and in Siberia, where the enhancement was delayed a few minutes from substorm onset. The oblique structure of the WEJ flowing poleward of the EEJ in the premidnight sector may be associated with a Harang discontinuity in this sector. The maximum negative disturbance of 560 nT was observed at PEL, which meant an enhancement of 300 nT in magnitude to the preexisting WEJ. By 2210 UT the maximum of the WEJ had shifted from

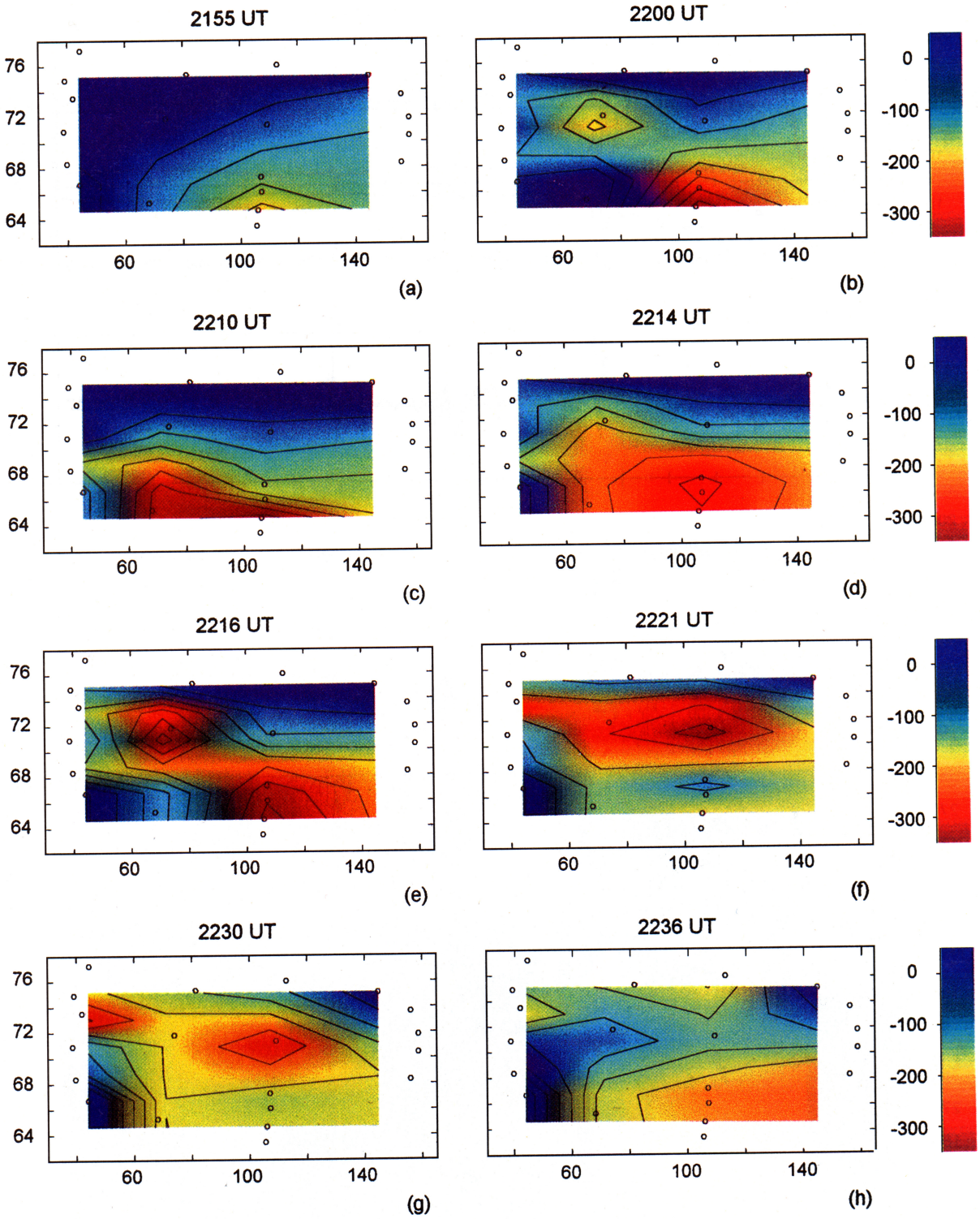

Plate 2. Surface plots of the north–south component of the magnetic disturbance in CGM coordinate system for selected time intervals. The color scale in units of nanoteslas is the same for each plot. Notice that the longitude and latitude axes are not in the same scale if measured in kilometers. Stations displayed by circles are from south to north as follows. Greenland west coast: NAQ, FHB, GHB, STF, ATU, UMQ; Greenland east coast and Iceland: LRV, SCO, DNB; Scandinavia: PEL, MUO, MAS, SOR, BJN, NAL; Siberia: DIK, IZV, UED, VIS, HEI. Substorm breakup S2 occurs between plots (a) and (b), intensification I2 between plots (c) and (d), intensification I3 between plots (e) and (f) and intensification I4 between plots (g) and (h).

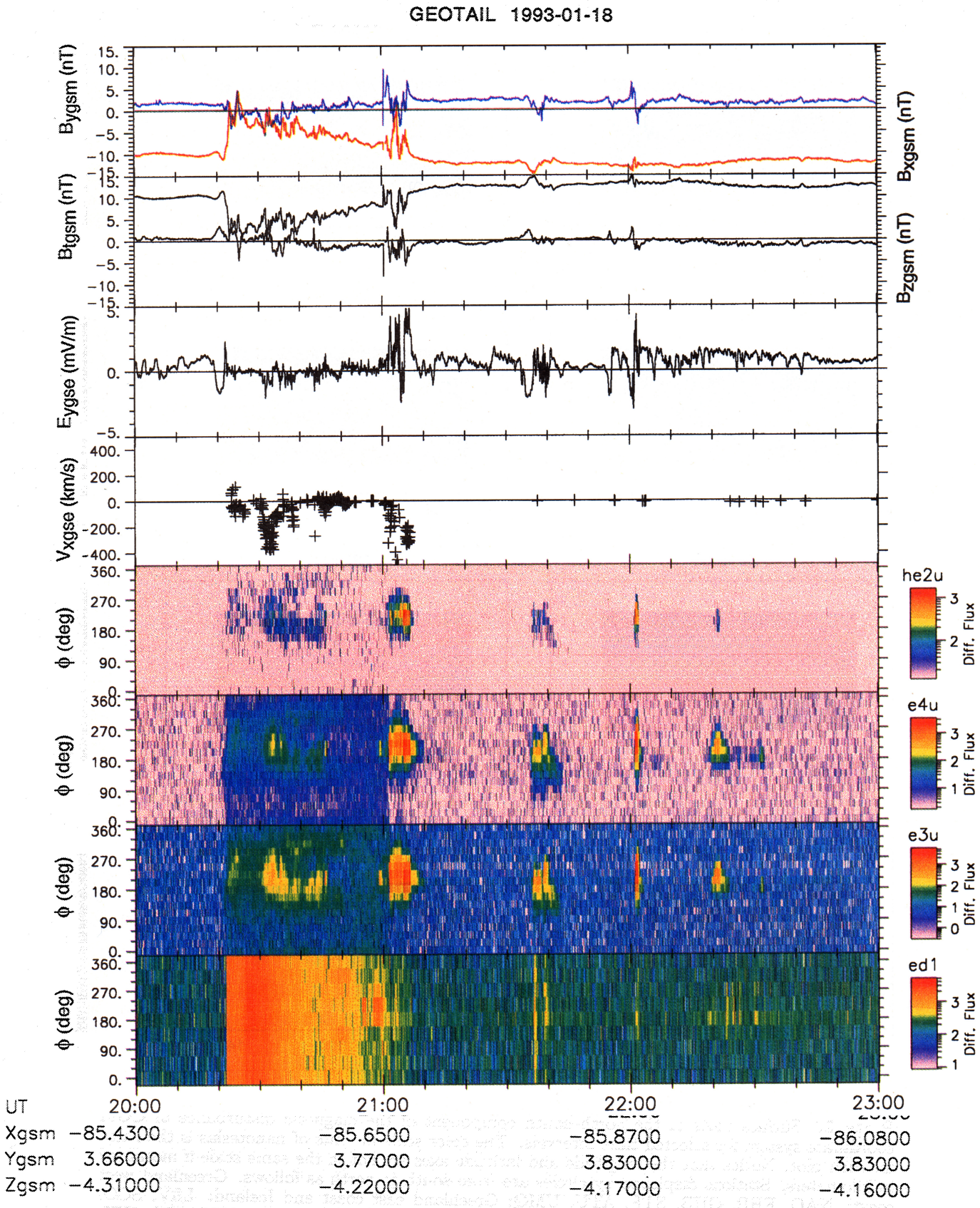

Plate 3. Geotail magnetic field, electric field and particle (EPIC instrument) data: (top to bottom) B_{ygsm}, B_{xgsm}, B_{tgsm} (total magnetic field), B_{zgsm}, E_{ygse}, V_{xgse}, he2 (helium, 70 - 96 keV), e4 (ions, 74 - 89 keV), e3 (ions, 62 - 74 keV), ed1 (electrons, > 34 keV).

the midnight sector to the preevening sector, possibly associated with a movement of the westward traveling surge (WTS) (Plate 2c).

At 2212 UT the WEJ intensity had decreased somewhat and the westward expansion had stopped. Then a substorm intensification (I2) started within the same MLT region as the substorm breakup (Plate 2d). On the Greenland west coast the WEJ started to increase at high latitudes ($\geq$ 71° CGMlat), but in Siberia, no change in currents occurred. The maximum current moved from the midnight to the pre–midnight sector in association with the westward moving fold (Figure 8) and the maximum negative bay of 580 nT was observed at SCO (Plate 2e).

At 2218 UT the current densities were decreasing. Then a new intensification (I3) of the WEJ started at about 71° - 72° CGMlat in Scandinavia and on the Greenland east coast. On the Greenland west coast the WEJ continued to increase slowly, the maximum current was flowing close to 73° CGMlat. Again, substorm intensification I3 had no effect on the currents in Siberia. At the maximum phase the negative bay at BJN reached 500 nT (Plate 2f). At that time the WEJ was split into two parts: the center of the high latitude portion was flowing at latitudes from 71° (midnight sector) to 73.5° CGMlat (evening sector) and the low latitude portion at 63° CGMlat. The currents corresponded to auroral regions in the KIL all–sky camera frame taken at 2221:43 UT in Figure 8, where a bright arc was located in the north, a dark area in the middle and diffuse aurora with some bright forms in the southern part of the sky.

At 2230 UT the gap between the split current system had been filled and a rather homogeneous WEJ was flowing in the region of diffuse aurora (Figs. 9 and 11g). Then a negative bay commenced at very high latitudes in the Scandinavian sector at NAL (76.0° CGMlat) and in Siberia at HEI (75.1° CGMlat) in association with substorm intensification I4. On the Greenland east coast at DNB (75.3° CGMlat) the WEJ continued to increase slowly and on the Greenland west coast the WEJ started to decrease, but the current was still significant at high latitudes. Again, a split WEJ current system formed and at the maximum phase the negative bays produced by the high and low latitude portions of the WEJ were 230 nT (at NAL) and 260 nT (at MAS), respectively (Plate 2h).

The poleward expansion of the WEJ is well documented in the midnight sector, where each intensification moved the current maximum approximately 4° CGMlat poleward as follows: S2 maximum occurs at PEL (63.4°), I2 maximum at SOR (67.2°), I3 maximum at BJN (71.3°), and I4 maximum at NAL (76.0°). The split WEJ formed during the last two intensifications probably corresponds to a feature known as a double oval [*Elphinstone et al.*, 1995].

The recovery phase started at different times at different local time sectors. In the evening sector (Greenland west coast) the WEJ at high latitudes started to decay at 2230 UT, in the premidnight sector (Greenland east coast) at 2245 UT and in the postmidnight (Scandinavia) and morning sectors (Siberia) at 2300 UT.

2.5.4. Geosynchronous particles. Geosynchronous particle data shows that the substorm breakup S2 was associated with a very pronounced injection of protons up to 470 keV at S/C 1987–097 (Figure 7). The onset time of the proton injection was 2157:20 UT and the location of the western boundary of the injection source region 20.4 MLT. The onset time of the electron injection at S/C 1984–129 was 2159:00 UT (Figure 3) and the location of the eastern boundary of the injection source region 2.5 MLT. The total width of the injection region was thus 6.1 MLT. The substorm intensifications occurring after the onset were not clearly visible in the geosynchronous particle data.

2.5.5. SCW locations. The substorm current wedge at the onset of substorm breakup S2 was estimated to be between 2156 and 2352 MLT (width 1.9 MLT), i.e. from the east coast of Greenland to the location of Geotail spacecraft at the magnetic midnight (Figure 5). The substorm breakup S2 extension is estimated to be 6 MLT by the geosynchronous data, 5.1 MLT by the ground high–latitude magnetic data and 1.9 MLT by the SCW estimate. Optical observations show that the onset took place westward of the Scandinavian sector, but the bulge expanded very rapidly in longitude, so the SCW estimate may best describe the width of the onset region just at the beginning of the event. The SCW locations have not been determined for substorm intensifications occurring after the substorm onset, since they occur at high latitudes and the current system is split.

2.6. Geotail Observations

The Geotail spacecraft was located close to the magnetic midnight at 23.9 MLT during the studied interval. The location of the spacecrafted changed from (−85.4, 3.7, −4.3) R_E to (−85.9, 3.9, −4.2) R_E during 2000 - 2200 UT in the GSM coordinate system. Geotail was located rather close to the tail center plane, so it was in a favorable position to observe plasmoids.

2.6.1. Plasmoid characteristics. The magnetic field within a plasmoid is closed on itself and the magnetic signature of a tailward moving plasmoid is a bipolar trace (north–then–south) in the B_z component. The original simple picture of plasmoids has proven to be inadequate on many occasions. Plasmoids do not generally exhibit a minimum in field intensity at their centers as would be expected for O-type neutral lines. Instead, a strong core field indicative of flux ropes is often present. Flux rope plasmoids can have a bipolar trace either in the north–south or east–west direction, suggesting a symmetry axis pointing along any orientation in the magnetotail [e.g., *Moldwin and Hughes,* 1991; *Slavin et al.,* 1995 and references therein].

The particle populations associated with plasmoids

can be divided into three categories: the plasmoid, the postplasmoid plasma sheet (PPPS) and the plasma sheet boundary layer (PSBL) populations [*Richardson and Cowley*, 1985; *Richardson et al.*, 1987]. The plasmoid contains isotropic energetic electrons (closed magnetic field lines) and a convecting energetic ion population. The PPPS, which is a wedge-shaped region of newly reconnected hot plasma on the earthward side of the plasmoid, typically contains an ion population convecting tailward faster than the plasmoid itself. The PSBL is a separatrix layer between the plasma sheet (PPPS or plasmoid) and the magnetic field mapping to the NENL.

When a plasmoid moves down the tail, it produces a several minute–long compression in the the lobe magnetic field. These events are called traveling compression regions, TCRs [*Slavin et al.*, 1993, 1994]. TCRs can be identified by (1) the aforementioned long compression in the field magnitude, (2) a typical, bipolar variation of the B_z component (north–then–south) with the inflection point coincident with the total field maximum, and (3) the persistent interval of B_z southward following the field compression. The variation in B_y may be either east–then–west or west–then–east and the B_x variation follows closely that of the total field magnitude.

Quite a few studies have been performed on the time delay between ground substorm onsets and plasmoid observations in the tail. *Nagai et al.* [1994] found that the time delays at $X_{gsm} \sim -80\ R_E$ of the bipolar B_z events from substorm onsets varied between 8 and 22 min. *Slavin et al.* [1993] found that the mean time delay of substorm onsets and TCRs at $X_{gsm} \sim -80\ R_E$ was 10 min, but the measured values ranged from 4 to 18 min.

In this study, plasmoids/flux ropes have been identified based on magnetic characteristics discussed above. Below we call all such measured magnetic structures as plasmoids. The observed plasmoids are related to ground onsets by the guideline that the expected delays at $X_{gsm} \sim -80\ R_E$ can vary from about 4 to 22 min. We take for the plasmoid observing time the center of the structure, which is the point where B_z changes sign for both the plasmoid and TCR signatures, as in previous studies.

2.6.2. Observations during the growth and expansion phases of the first substorm. Plate 3 shows the Geotail magnetic field, electric field, inferred plasma flow velocity and energetic particle data during the entire time interval studied. Figure 10 shows in more detail the variations of the magnetic field components from 2010 to 2110 UT. The bottom panel displays the convective flow velocity of the plasma in the X_{gse} direction. It is computed from E_{ygse} and the magnetic field components for times that the magnetic field points in a direction that the most significant contribution to V_{xgse} is from E_{ygse} (for details of the computation, see *Angelopoulos et al.* [1996b]). Note, that the actual flow velocity along the X_{gse} direction may be greater, since the inferred velocity is the $\perp \vec{B}$ component of the velocity in the X_{gse} direction and in the studied cases a field–aligned component of the plasma flow may be significant.

At 2022 UT, Geotail enters deep in a plasmoid, as evidenced by the decrease of the total magnetic field intensity and the increase in the fluxes of energetic electrons and ions (Plate 3). Energetic electrons are very isotropic confirming the closed character of the field lines. Ions show a tailward anisotropy consistent with a tailward flow. Below the magnetic field signatures (Figure 10) of the events are described, and the observing time of the center of the magnetic structure relative to the ground onset time of events is given.

1. P1 + 18.5 min corresponding to time interval of 2022 - 2026 UT. The event shows the north–then–south variation in B_z, which is associated with the east–then–west variation in B_y. The tailward plasma velocity is quite low, about 80 km s^{-1}, which might indicate that the plasmoid associated with pseudobreakup P1 is quasi-stagnant. The long time delay between the ground onset and the plasmoid detection supports the interpretation.

2. P2 + 9.5 min corresponding to time interval of 2030 - 2037 UT. There is a large–scale variation in B_z north–then–south, which contains a lot of substructure. B_y is mainly toward east. The tailward plasma velocity is initially small, but reaches 400 km s^{-1} between 2031:00 and 2033:30 UT, whereafter it decreases again. Associated with this event, the flux of tailward moving ions increases, which is consistent with the increase of tailward convection velocity. We connect this plasmoid with pseudobreakup P2.

3. Time interval of 2037 - 2100 UT. The B_z has a positive (northward) peak 2037 - 2039 UT, during which the tailward velocity reaches 200 km s^{-1}. This peak may belong to the plasmoid associated with pseudobreakup P2. After 2039 UT B_z remains negative excluding two weak positive peaks at 2043 and 2046 UT, which are transient current filaments that are unlikely to contribute to the large scale dynamics of the tail. The tailward velocity is small. We associate this time period to a postplasmoid plasma sheet (PPPS) phase, although the flow velocity is small. Probably, the plasmoid associated with pseudobreakup P2 was not followed by a strong plasma sheet reconnection.

4. S1 + 10.5 min corresponding to time interval of 2100 - 2109 UT. The magnetic signatures associated with substorm breakup S1 are very complicated. The long duration of the disturbances make it possible that some of them may be related to the substorm intensification I1, which occurs 8 min after substorm breakup S1. The tailward velocity during 2101 - 2102 UT is about 200 km s^{-1}, the velocity peaks between 2103 and 2104 UT when it reaches 800 km s^{-1} and during 2105:30 - 2106:30 UT the velocity varies between 200 and 600 km s^{-1}. We take the center of the event to be

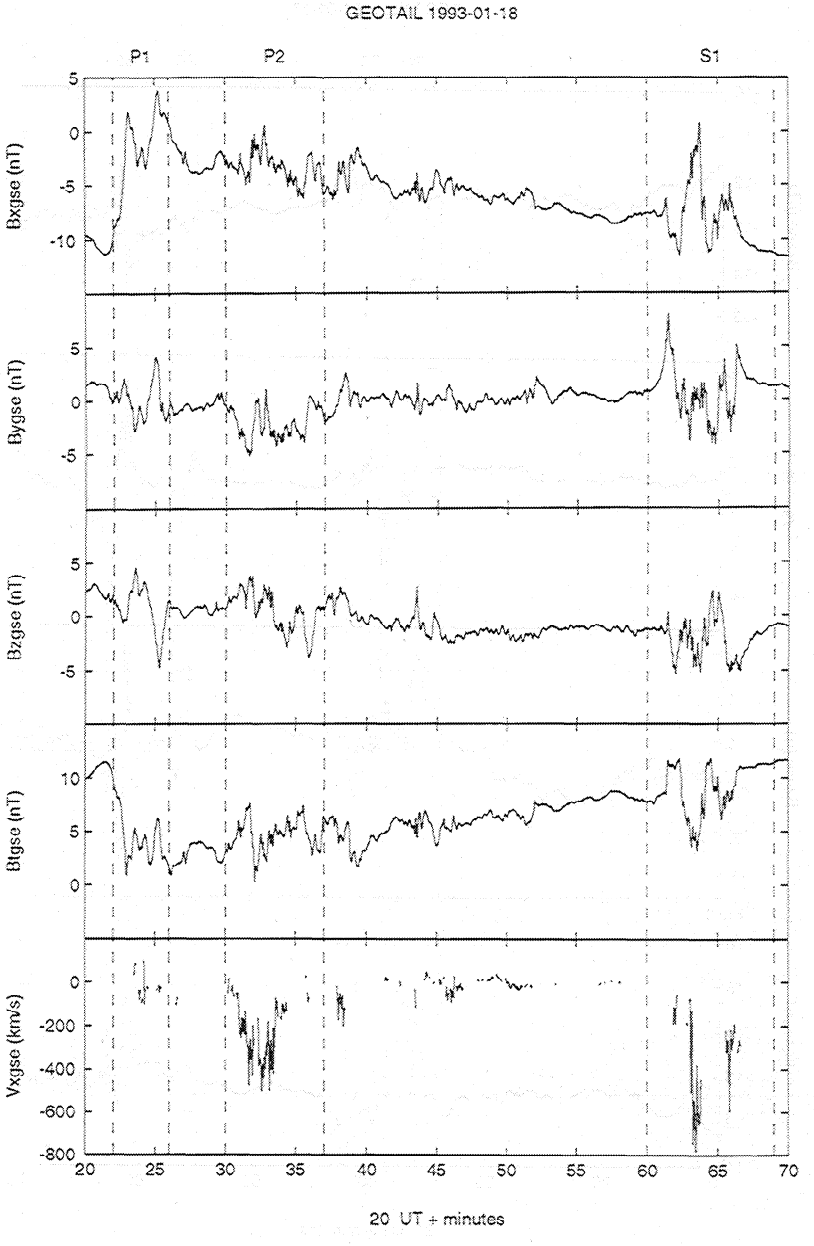

Figure 10. Geotail magnetic field components and calculated convective flow velocity in the X_{gse} direction for the time interval of 2020 - 2110 UT.

2103:30 UT when maximum tailward flow is measured.

The particle signatures preceeding the plasmoid associated with substorm breakup S1 are tailward electron beams commencing at 2054:50 and 2057:30 UT and tailward ion beams at 2058:40 and 2101:20 UT (Plate 3). If we assume that the 2054:50 UT electron beam and the 2058:40 UT ion beam are associated with the same acceleration process closer to the Earth, we arrive at an onset time of 2054:42 UT and a distance of 133 R_E. The distance is too large (Geotail location is -86 R_E) indicating that the time difference between the electron and ion beams is not just due to the time–of–flight effect. Possible reasons are spatial effects [*Richardson and Cowley,* 1985], the non–zero pitch angles of the measured protons and the finite time constant of the reconnection pulse. The observations indicate that in less than 2 min from substorm breakup (2053 UT) reconnection reached field lines mapping to Geotail, which obviously were open field lines. The time delay between the 2057:30 UT electron beam and the 2101:20 UT proton beam is the same (230 s) as in the previous case, but the ion distributions may be modified by the enhanced convection after 2101 UT.

2.6.3. Observations during the growth and expansion phases of the second substorm. Figure 11 shows the variations of the magnetic field components from 2110 to 2210 UT. The negative B_x component indicates that Geotail is located south of the neutral sheet. The B_z component is also negative, which may be related to the PPPS, though the tailward ve-

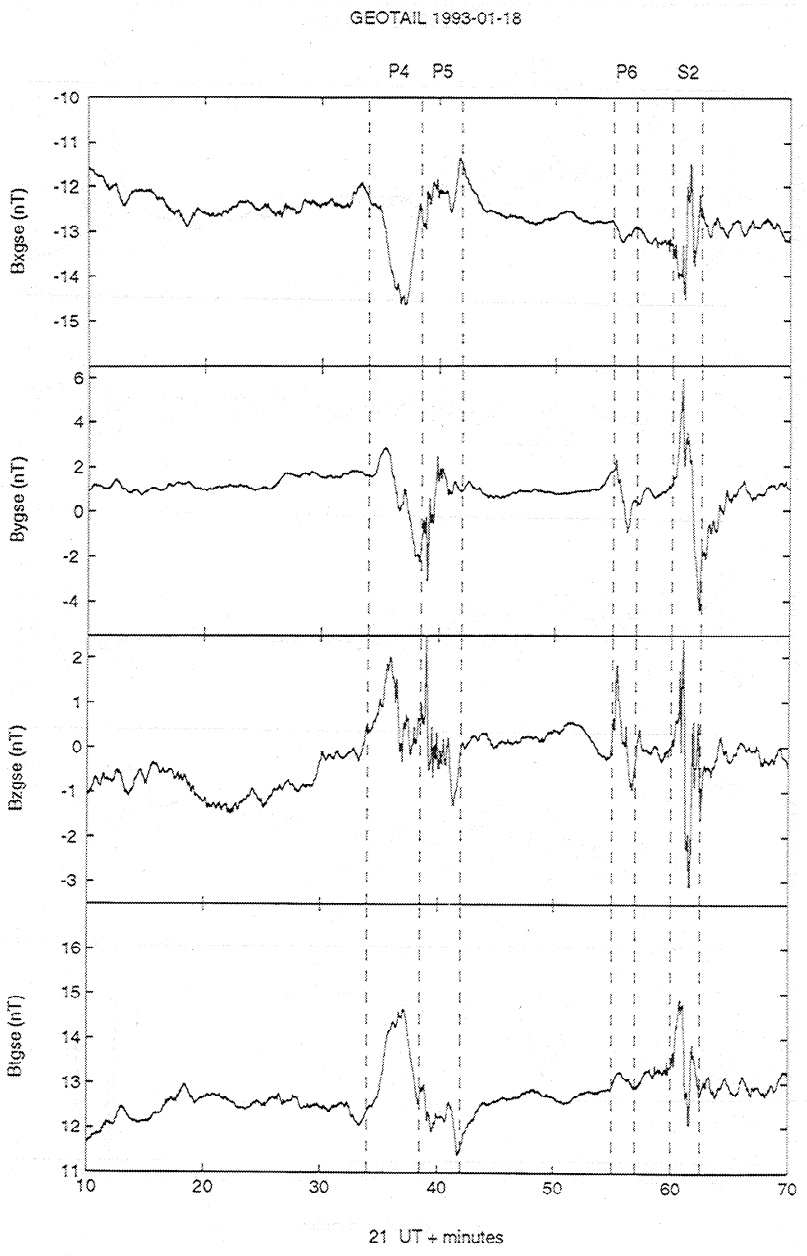

Figure 11. Geotail magnetic field components for the time interval of 2110 - 2220 UT.

locity is low, or the tilting of the whole plasma sheet due to a solar wind effect.

The magnetic signatures after 2110 UT could be interpreted as TCRs and most of them were accompanied by energetic particle enhancements, suggesting grazing of the outer boundary of the associated plasmoid. Since TCR signatures are very similar to a crossing of an outer boundary of a plasmoid, we don't make any clear distinction between these two cases.

There are three clear events after 2110 UT in the Geotail magnetic field.

1. P4 + 9.5 min corresponding to time interval of 2134:00 - 2138:30 UT, maximum compression at 2136:30 UT. B_z changes north–then–south and B_{tot} is compressed from 12.1 to 14.8 nT (22 %). B_y changes east–then–west. We associate this plasmoid with pseudobreakup P4.

2. P5 + 6 min corresponding to time interval of 2138:30 - 2142:00 UT, maximum compression at 2139:00 UT. There is again a north–then–south change in B_z, which is accompanied by a small local increase in B_{tot} ($\leq$ 8 %). This event is associated with pseudobreakup P5, which also on the ground follows event P4 with no separation. Both of the magnetic structures P4 and P5 are associated with a passage of the outer part of a plasmoid, since tailward ion beams are observed starting at about 2136 and 2139 UT in association with simultaneous isotropic electron fluxes (Plate 3).

3. P6 + 7 min corresponding to time interval of 2155 - 2157 UT, maximum at 2156 UT. Though small in am-

plitude, this event shows the classical features of a TCR: B_z north–then—south and B_{tot} compression (3.5%). B_y changes east–then–west. No particle signatures are associated with this event. This TCR is related to pseudobreakup P6, which also on the ground produces only small disturbances.

4. S2 + 5 min corresponding to time interval of 2200:00 - 2202:30 UT, maximum compression of B_{tot} (11 %) at 2201 UT. This event is related to a passage of the outer edge of a complicated magnetic structure occuring in association with substorm breakup S2. Short-duration simultaneous electron (rather broad angle) and proton tailward beams are observed at 2201 UT.

Plate 3 displays a tailward ion (62 - 74 keV) beam at 2219:30 UT, which is preceeded (followed) by an electron (He) beam. This particle injection is plausibly associated with substorm intensification I3. Weak dispersed particle beams are observed also around 2230 UT, associated with substorm intensification I4. These events are not associated with magnetic structures and we interpret them as acceleration of energetic particles by reconnection occuring Earthward of Geotail.

2.6.4. Comparison of Geotail observations to ground and geosynchronous observations. There are at least four means to define the ground onset time of events: (1) midlatitude Pi2 pulsation trains, (2) auroral zone PiB pulsations, (3) auroral brightenings and (4) high latitude negative bays. Signatures (2), (3) and (4) are local, whereas midlatitude Pi2s in the nightside ionosphere are not, though also them suffer from some limitations [e.g., *Yeoman et al.*, 1994]. That is why the onset time was defined based on Pi2 onsets. Since the very high latitude intensifications I2 - I4 did not produce midlatitude Pi2s, possibly due to the screening effect of the very disturbed ionosphere, the onset time of these events were defined by signature (4). The onset times agreed usually within one minute between signatures (1) and (2) and within 2 min when all signatures were considered. The same signature (1) was used to define the duration of the events, since for the cases where signatures (1) - (3) could be utilized together it was shown that the duration of Pi2s correlated well with the duration of PiB activity and auroral brightenings. This observation is in agreement with the suggestion by *Singer et al.* [1988] that while the near-tail reconnection continues, Alfvén waves and subsequently midlatitude Pi2s are continuously generated. Because of the lack of Pi2s, the durations of events after substorm breakup S2 were determined to be the separations of substorm intensifications from each other.

The results of ground–Geotail comparison are summarized in Table 2, which clearly demonstrates that the majority of the events observed on the ground and at the geosynchronous altitude are also observed in the midtail. The time delay between the plasmoid observation (center of the structure) and ground onset is typically about 10 min, the longest delay of 18.5 min is observed for pseudobreakup P1 and the shortest delay of 5 min for the substorm breakup S2. The differences may be related to the variable velocities at which the plasmoids move down the tail and to the different starting points in the X_{gsm} direction. Injected electron beams are observed almost simultaneosly with ground onset for substorm intensifications I3 and I4, whereas for the substorm breakup S1 there is a delay of less than 2 min.

Table 2. Comparison Between Ground Onset Times and Midtail Observations of Plasmoids, Traveling Compression Regions (TCRs) or Particle Beams

Event	UT_0	G_m, UT	G_e, UT	$G_m - UT_0$	ΔMLT
P1	2006	2024:30		18:30	0038
P2	2024	2033:00		9:30	0029
P3	2044				0018
S1	2053	2103:30	2054:50	10:30	-0001
			2057:30		
I1	2101				
P4	2127	2136:30		9:30	-0034
P5	2134	2140:15		6:12	-0040
P6	2149	2156:00		7:00	-0054
S2	2156	2201:00		5:00	-0059
I2	2212				
I3	2218		2218:20		-0116
I4	2230		2230:00		-0128

UT_0 is onset time determined by ground observations, G_m time of plasmoid center at Geotail determined from magnetic observations, G_e onset time of energetic electron beam with no simultaneous magnetic structure at Geotail, ΔMLT difference between Geotail location (23.9 MLT) and the IMAGE chain.

Geotail observations of plasmoids or TCRs or accelerated particle beams using the onset times of the events on the ground according to Table 2 are marked by squares in Figure 5. Geotail location close to magnetic midnight (23.9 MLT) is favorable to see all the events provided that the plasmoid extent in azimuth in the midtail corresponds to the current disruption region in the ionosphere. This assumption seems to hold, since only events P3 and I2 are clearly missed. (It is possible that magnetic structures related to substorm breakup S1 cover also substorm intensification I1.) In addition, the Geotail data indicates that the western edge of substorm intensification I4 is located between the Geotail footpoint and the east coast of Greenland. The reason for missing events P3 and I2 may be either in the localization of these events in the Y_{gsm} or Z_{gsm} direction. However, in the case of a small scale in the Z_{gsm} direction, signatures of TCRs should have been expected. A more probable explanation is the longitudinal localiza-

Table 3. Summary of the Characteristics of Pseudobreakups (P), Substorm Breakups (S) and Substorm Intensifications (I)

Event	Duration, min	Expansion, deg	Extent, MLT			SCW, MA	Disturbance, nT		Midtail
			SCW	INJ	MAG		Total	Change	
P1	14	0.7	1.9			0.12	-50	-30	P
P2	12	0.0[a]	4.5			0.09	-170	-150	P
P3	5	0.0[a]	3.0			0.21	-450	-330	-
S1	8	4.0	1.3			0.19	-520	-420	P
I1	8	3.5	5.7	3.3	2.9	0.34 (0.53)[b]	-800	-700	P
P4	7	0.0	1.3			0.26	-380	-190	T
P5	5	1.2		3.0	2.5	0.11	-460	-120	T
P6	5	0.0	2.0		2.5	0.05	-320	-90	T
S2	16	3.6	1.9	6.1	5.1	0.50	-560	-300	T
I2	6	3.8			5.1	0.16 (0.66)[b]	-580	-500	-
I3	12	3.9			2.5	0.05	-500	-430	B
I4	10	4.7			2.9	0.02	-240	-180	B

The columns from left to right are as follows: event, duration, the amount of poleward expansion, the extent of the (1) substorm current wedge (SCW), (2) geosynchronous altitude injection region (INJ) and (3) high latitude magnetic disturbance (MAG) at onset, the intensity of the SCW, the maximum disturbance of the high latitude magnetic north components from the quiet level (total) and from the start of the activation (change) and midtail observations of plasmoids (P), TCRs/outer edges of plasmoids (T) or particle beams without associated magnetic signatures (B).

[a]Estimated in the Scandinavian sector.

[b]Value measured from the substorm (S1 or S2) onset baseline instead of the start of the activation.

tion. The B_y component of the IMF may distort the mapping of Geotail location to the ground so that actually Geotail maps outside of the SCW region during events P3 and I2.

3. Summary

Table 3 presents a summary of the observed features of pseudobreakups, substorm breakups and substorm intensifications. We defined those short-lived events as pseudobreakups, which were not associated with a significant ($> 2°$) poleward expansion. In this study we concentrated only on the large scale features of the events, though many of the studied signatures (e.g., auroral intensifications, injections and plasmoids) exhibited temporal substructure.

3.1. Duration of the Events

The onset time and event length estimate has been made mainly by using midlatitude Pi2 magnetic pulsation data (see the previous section). As can be seen from the values presented in Table 3, the durations of the events cannot be used to separate pseudobreakups (5 - 14 min) from substorm breakups (8 - 16 min) or substorm intensifications (6 - 12 min). Even when the total length of the first substorm expansion phase including breakup S1 and the ensuing intensification I1 is considered (16 min), no significant difference from the durations of some pseudobreakups is evident. The expansion phase of the second substorm includes the substorm S2 breakup and the three intensifications (I2 - I4), and its total duration (44 min) exceeds markedly that of any pseudobreakup.

3.2. Poleward Expansion

The amount of poleward expansion for the events have been estimated based on optical or magnetic data and this feature was used to classify the events. In these cases, the amount of poleward expansion was 0 - 1.2° for pseudobreakups, 3.6 - 4.0° for substorms and 3.5 - 4.7° for substorm intensifications.

3.3. Localization of the Events

The extents of the events are shown in Figure 5 and in Table 3. The SCW estimates at the onset of the events ranged from 1.3 to 4.5 MLT for pseudobreakups, from 1.3 to 1.9 MLT for substorm breakups and a value of 5.7 MLT was found for substorm intensification I1. Only three injection region width estimates were possible to make and values ranged between 3.0 and 6.1 MLT. A distinct difference is found between the

width of substorm S2 estimated by the SCW calculation (1.9 MLT) and drift of injected particles (6.1 MLT). We suggest that the width is small at the onset, but expands rapidly in azimuth, which affects the geosynchronous orbit observations. Event widths were also estimated on the basis of commencements of high latitude negative bays. This method gave the most crude estimates, since only four different longitudinal chains with separations ranging between 2.5 and 2.9 were available. Taken the results together, we find no significant difference in the widths between pseudobreakups and substorm breakups, but the substorm intensifications seem to be associated with somewhat larger values (of the order of 5 - 6 MLT). This is expected, since substorm intensifications are associated with further expansion of the substorm current wedge in longitude and latitude.

3.4. Intensity of the Events

The total intensity of the SCW current was estimated on the basis of midlatitude magnetograms. The largest value (0.5 MA) was associated with substorm breakup S2 and each subsequent intensification increased the total current intensity. Derived current intensities were 0.05 - 0.26 MA for pseudobreakups, 0.19 - 0.50 MA for substorm breakups and 0.02 - 0.34 MA for substorm intensifications.

The horizontal distribution of the total current flowing determines the magnetic disturbances at high latitude stations. The magnitude of high–latitude negative bays as measured from the quiet time baseline (total value) and from the level at the start of the activation (differential value) are shown in Table 3. The magnitudes of differential negative bays varied from 30 to 330 nT for pseudobreakups, from 300 to 420 for substorm breakups and from 180 to 700 for substorm intensifications. In general, pseudobreakups produced smaller disturbances than substorm breakups and intensifications. However, there is a wide range of pseudobreakups from very weak to intense events and no distinct values can be set to current or disturbance levels to separate pseudobreakups from substorm breakups.

3.5. Auroral Features

Auroral features were recorded in Scandinavia, which was located in the midnight sector. Pseudobreakups P1 - P4 and P6 were associated with brightenings of arcs. Pseudobreakup P5 was associated with a surge, which differed from the substorm–associated westward traveling surge (WTS) in many respects. Pseudobreakup surges are discussed previously by *Akasofu* [1964] and *Nakamura et al.* [1994]. The substorm S1 breakup occuring to the east of Scandinavia was followed by an appearance of a classical WTS. The onset of substorm breakup S2 occurred to the west of Scandinavia and it was followed by an eastward and poleward expanding bulge. Substorm intensifications I1 - I4 were associated with an intensification of an arc located at the poleward boundary of the bulge and further poleward expansion of aurora and the associated currents. In addition, intensifications I2 and I3 were associated with a formation of a large–scale fold, which drifted westward along the arc. A split westward electrojet was forming during intensifications I3 and I4.

3.6. Magnetospheric Configuration Changes

Geotail observations in the midtail are summarized in Tables 2 and 3. Pseudobreakups P1 and P2 and substorm breakup S1 were associated with observations of plasmoids at the location of Geotail ($X_{gsm} \sim -86\ R_E$). The time delays between ground onsets and midtail observations of plasmoids varied between 9.5 and 18.5 min. After the first substorm TCRs/outer boundaries of plasmoids were observed at Geotail. The time delays of observed TCRs from the onset of the events ranged from 5.0 to 9.5 min. For substorm intensifications I3 and I4 dispersed particle beams without following magnetic signatures were observed and they were interpreted as injections of particles by reconnection occurring earthward of Geotail. Only two ground events (P3 and I2) were associated with no signatures of reconnection at Geotail, possibly due to a localization of the events in the Y_{gsm} direction.

3.7. Summary

Several mechanisms have been proposed for the initiation of substorm expansion. Almost all of them result at least in one of the following processes: the cross–tail current disruption or the near–Earth neutral line (NENL) formation. The temporal and causal relationship between these processes is a subject of continuing debate [see, e.g., *Kennel*, 1992; *McPherron and Fairfield*, 1998]. The current disruption is believed to take place rather close to Earth, at the inner edge of the plasma sheet, whereas the reconnection occurs between $X_{gsm} \sim -20$ and $-30\ R_E$, according to recent Geotail observations [*Nagai et al.*, 1998]. This study shows that all substorms, substorm intensifications and even weakest pseudobreakups are associated with both processes: cross–tail current disruption evidenced by the SCW formation and near–Earth reconnection evidenced by a plasmoid release.

4. Conclusions

By considering a number of short-lived activations with a limited poleward expansion (pseudobreakups) which occurred either during a substorm growth phase or between two distinct substorms, we found that there is no definitive qualitative difference between pseudobreakups and substorm breakups. Both kinds of activations showed distinct reconnection signatures at $X_{gsm} \sim -86\ R_E$ and were associated with substorm current wedge formation, midlatitude magnetic Pi2 pulsations and particle injection at the geosynchronous orbit. We

conclude that there is a continuum of states between the small pseudobreakups and large substorms but no specific value of current, extent, duration of activation, etc. which distinguish between these two.

The events that we normally call as substorms are often a superposition of many breakups (here we have called events immediately following substorm breakups as substorm intensifications), each of which is responsible for a further expansion of the disturbed region in the ionosphere. It is not clear from this study why pseudobreakups remain isolated events. Previous studies have evoked several candidates for regulating the initiation and development of substorms: (1) the magnetosphere-ionospheric coupling [*Kan et al.*, 1988], (2) local magnetospheric conditions [e.g., *Baker et al.*, 1996; *Lui*, 1998] and (3) solar wind-magnetosphere coupling [e.g., *Lyons*, 1996]. This study do not lend credence to candidate (1), since EISCAT measurements of conductivities in the auroral oval before the two substorms don't show any evidence of the change in conditions before substorms at least in the vicinity of the radar. The question of the factors which trigger and quench the instability producing the breakups is left for future studies.

Acknowledgments. The authors thank T. Bösinger and T. Lui for useful discussions. We thank K. Tsuruda for the EFD instrument data from Geotail. The contribution of the magnetic field data from the MGF instrument on the Geotail spacecraft by S. Kokubun is greatfully acknowledged. We are grateful to the JHU/APL EPIC team for providing us the energetic particle data from Geotail. We thank D. K. Milling and D. Orr for the SAMNET data. SAMNET is a PPARC facility deployed and operated by the University of York. Thanks are due to Friis–Christensen and T. Moretto for the data of the Greenland Magnetometers of the Danish Meteorological Institute. The Ny Aalesund, Bear Island and Leirvogur data were obtained through the WDC-A, we thank L. Morris for providing us the data. We acknowledge L. Häkkinen from the Finnish Meteorological Institute for providing the IMAGE data. The IMAGE magnetometer network is jointly operated by the Technical University of Braunschweig, the Finnish Meteorological Institute, the Geo-Sciences-Center, Potsdam, and the Sodankylä Geophysical Observatory. We thank A. Kotikov and E. Shishkina for the KARA magnetic chain data. We thank K. Kaila for the optical measurements and data provided during the EISCAT campaigne and K. Kauristie from the Finnish Meteorological Institute for providing us the all–sky camera data from KIL and MUO. The EISCAT scientific association is supported by Suomen Akatemia (Finland), Centre Nationale de la Recherche Scientifique (France), Max–Planck-Gesellschaft (F.R.G.), Norges Almenvitenskapelige Forskningsråd (Norway), Naturvetenskapliga Forskningsrådet (Sweden) and the Scientific and Engineering Research Council (U.K.). The work by ATA has been supported by the Academy of Finland and the work by VAS, MAS, and LIV by the RFBR grant N 98-05-04114.

Michel Blanc thanks both referees for their assistance in evaluating this paper.

References

Aikio, A. T., and K. U. Kaila, A substorm observed by EISCAT and other ground-based instruments – Evidence for near-Earth substorm initiation, *J. Atmos. Terr. Phys.*, *58*, 5 - 21, 1996.

Akasofu, S.–I., The development of the auroral substorm, *Planet. Space Sci.*, *12*, 273 - 282, 1964.

Angelopoulos, et al., Multipoint analysis of a bursty bulk flow event on April 11, 1985, *J. Geophys. Res.*, *101*, 4967 - 4989, 1996a.

Angelopoulos, V., V. A. Sergeev, F. S. Mozer, K. Tsuruda, S. Kokubun, T. Yamamoto, R. Lepping, G. Reeves, and E. Friis–Christensen, Spontaneous substorm onset during a prolonged period of steady, southward interplanetary magnetic field, *J. Geophys. Res.*, *101*, 24583 - 24589, 1996b.

Baker, D. N., T. I. Pulkkinen, V. Angelopoulos, W. Baumjohann, and R. L. McPherron, Neutral line model of substorms: Past results and present view, *J. Geophys. Res.*, *101*, 12975 - 13010, 1996.

Bösinger, T., K. Alanko, J. Kangas, H. Opgenoorth, and W. Baumjohann, Correlations between PiB type magnetic micropulsations, auroras and equivalent current structures during two isolated substorms, *J. Atmos. Terr. Phys.*, *9*, 933 - 945, 1981.

Elphinstone, R. D., et al., The double oval auroral distribution, 2., The most poleward arc system and the dynamics of the magnetotail, *J. Geophys. Res.*, *100*, 12093 - 12102, 1995.

Hones, E. W., Jr., Transient phenomena in the magnetotail and their relation to substorms, *Space Sci. Rev.*, *23*, 393, 1979.

Kan, J. R., L. Zhu, and S.-I. Akasofu, A theory of substorms: Onst and subsidence, *J. Geophys. Res.*, 93, 5624, 1988.

Kennel, C. F., The Kiruna conjecture: The Strong version, *Proceedings of the First International Conference on Substorms, Kiruna, Sweden, 23 - 27 March 1992, Eur. Space Agency Spec. Publ., SP-335*, 599 - 601, 1992.

Koskinen H. E. J., R. E. Lopez, R. J. Pellinen, T. I. Pulkkinen, D. N. Baker, and T. Bösinger, Pseudobreakup and substorm growth phase in the ionosphere and magnetosphere, *J. Geophys. Res.*, *98*, 5801 - 5813, 1993.

Lui, A. T. Y., Synthesis (current disruption) model for substorms, in *Substorms-4, International Conference on Substorms-4, Lake Hamana, Japan, March 9 - 13, 1998*, edited by S. Kokubun and Y. Kamide, pp. 361 - 366, Kluwer Acad., Norwell, Mass., 1998.

Lyons, L. R., Substorms: Fundamental observational features, distinction from other disturbances, and external triggering, *J. Geophys. Res.*, *101*, 13011 - 13025, 1996.

McPherron, R. L., Magnetospheric substorms, *Rev. Geophys. Space Phys.*, *17*, 657 - 671, 1979.

McPherron, R. L., Physical processes producing magnetospheric substorms and magnetic storms, in *Geomagnetism*, vol. 4, edited by J. A. Jacobs, p. 593, Academic, San Diego, Calif., 1991.

McPherron, R. L., and D. H. Fairfield, Session 1 Summary: What are the major expansion phase actions as seen at various regions, in *Substorms-4, International Conference on Substorms-4, Lake Hamana, Japan, March 9 - 13, 1998*, edited by S. Kokubun and Y. Kamide, pp. 29 - 33, Kluwer Acad., Norwell, Mass., 1998.

Moldwin, M. B., and W. J. Hughes, Plasmoids as flux ropes, *J. Geophys. Res.*, *96*, 14051 - 14064, 1991.

Nagai, T., K. Takashi, H. Kawano, T. Yamamoto, S. Kokubun, and A. Nishida, Initial GEOTAIL survey of magnetic substorm signatures in the magnetotail, *Geophys. Res. Lett.*, *21*, 2991 - 2994, 1994.

Nagai, T. M. Fujimoto, Y. Saito, S. Machida, T. Terasawa, R. Nakamura, T. Yamamoto, T. Mukai, A. Nishida, and S. Kokubun, Structure and dynamics of magnetic reconnection for substorm onsets with Geotail observations, *J. Geophys. Res.*, *103*, 4419 - 4440, 1998.

Nakamura, R., D. N. Baker, T. Yamamoto, R. D. Belian, E. A. Bering III, J. R. Benbrook, and J. R. Theall, Particle and field signatures during pseudobreakup and major expansion onset, *J. Geophys. Res.*, *99*, 207 - 221, 1994.

Ohtani, S., et al., A multisatellite study of a pseudo-substorm onset in the near–Earth magnetotail, *J. Geophys. Res.*, *98*, 19355 - 19367, 1993.

Petrukovich, A. A., et al., Two spacecraft observations of a reconnection pulse during an auroral breakup, *J. Geophys. Res.*, *103*, 47 - 59, 1998.

Pulkkinen, T. I., Pseudobreakup or substorm?, in *Proceedings of the 3. International Conference on Substorms, May 13 - 17, 1996, Versailles, France, Eur. Space Agency Spec. Publ., SP–389*, 285 - 293, 1996.

Richardson, I. G., and S. W. H. Cowley, Plasmoid-associated energetic ion bursts in the deep geomagnetic tail: Properties of the boundary layer, *J. Geophys. Res.*, *90*, 12133 - 12157, 1985.

Richardson, I. G., S. W. H. Cowley, E. W. Hones Jr., and S. J. Blame, Plasmoid-associated energetic ion bursts in the deep geomagnetic tail: Properties of plasmoids and the postplasmoid plasma sheet, *J. Geophys. Res.*, *92*, 9997 - 10013, 1987.

Rostoker, G., S.–I. Akasofu, J. Foster, R. A. Greenwald, Y. Kamide, K. Kawasaki, A. T. Y. Lui, R. L. McPherron, and C. T. Russel, Magnetospheric substorms – Definition and signatures, *J. Geophys. Res.*, *85*, 1663 - 1668, 1980.

Sergeev, V. A., L. I. Vagina, R. D. Elphinstone, J. S. Murphree, D. J. Hearn, L. L. Cogger, and M. L. Johnson, Comparison of UV optical signatures with the substorm current wedge as predicted by an inversion algorithm, *J. Geophys. Res.*, *101*, 2615 - 2627, 1996.

Singer, H. J., E. W. Hones Jr., and T. J. Rosenberg, Multipoint measurements from substorm onset to recovery: The relation between magnetic pulsations and plasma sheet thickening, *Adv. Space Res.*, *8* (9), 443 - 446, 1988.

Slavin, J. A., M. F. Smith, E. L. Mazur, D. N. Baker, E. W. Hones Jr., T. Iyemori, and E. W. Greenstadt, ISEE 3 Observations of traveling compression regions in the Earth's magnetotail, *J. Geophys. Res.*, *98*, 15425 - 15446, 1993.

Slavin J. A., C. J. Owen, and M. Hesse, Evolution of the plasmoid-lobe interaction with downtail distance, *Geophys. Res. Lett.*, *21*, 2765 - 2768, 1994.

Slavin J. A., C. J. Owen, M. M. Kuznetsova, and M. Hesse, ISEE 3 observations of plasmoids with flux rope magnetic topologies, *Geophys. Res. Lett.*, *22*, 2061 - 2064, 1995.

Vagina, L. I., V. A. Sergeev, D. N. Baker, and H. J. Singer, Use of mid-latitude magnetic data for modelling and diagnostics of magnetospheric substorms, *Adv. Space Res.*, *18* (8), 229 - 232, 1996.

Yeoman, T. K., M. P. Freeman, G. D. Reeves, M. Lester, and D. Orr, A comparison of midlatitude Pi 2 pulsations and geostationary orbit particle injections as substorm indicators, *J. Geophys. Res.*, *99*, 4085 - 4093, 1994.

A. T. Aikio, Department of Physical Sciences, University of Oulu, P.O. Box 3000, FIN–90401 Oulu, Finland. (Anita.Aikio@oulu.fi)

V. Angelopoulos, Space Sciences Laboratory, University of California, Berkeley, Berkeley, CA 94720-7450

G. Reeves, Los Alamos National Laboratory, Los Alamos, NM 87545

V.A. Sergeev, M. A. Shukhtina, and L. I. Vagina, Institute of Physics, University of St. Petersburg, St. Petersburg, 198904, Russia

(Received August 25, 1998; revised December 18, 1998; accepted January 23, 1999.)